**Tracing the cellular origins of mesenchymal derivatives in craniofacial development**

by

Kathleen Anne Martin

DDS, Western University, 2015

BSc, Queen's University, 2011

A THESIS SUBMITTED IN PARTIAL FULFILLMENT OF
THE REQUIREMENTS FOR THE DEGREE OF

MASTER OF SCIENCE

in

THE FACULTY OF GRADUATE AND POSTDOCTORAL STUDIES

(Craniofacial Science)

THE UNIVERSITY OF BRITISH COLUMBIA

(Vancouver)

August 2018

**COMMITTEE PAGE**

The following individuals certify that they have read, and recommend to the Faculty of Graduate and Postdoctoral Studies for acceptance, a thesis/dissertation entitled:

**Tracing the cellular origins of mesenchymal derivatives in craniofacial development**

---

submitted by: Kathleen Martin in partial fulfillment of the requirements for

the degree of: Master of Science

in: Craniofacial Science (Orthodontics)

## Examining Committee:

Dr. T. Michael Underhill
Supervisor

Dr. Timothy O'Connor
Supervisory Committee Member

Dr. Edward Putnins
Supervisory Committee Member

Dr. Siddharth Vora
Additional Examiner

**ABSTRACT**

**Objectives:** Numerous genes have been shown to impact craniofacial development. One such gene, *Hypermethylated in cancer 1* (*Hic1*), is a tumour suppressor gene that encodes for the transcription factor HIC1. *Hic1* is broadly expressed within embryonic mesenchyme. *Hic1* knockout mice demonstrate multiple craniofacial anomalies, including facial clefting, abnormal closure/truncation of the secondary palate, low-set/underdeveloped ears, abnormal eye development, shortened snouts, acrania, and exencephaly, suggesting a role for *Hic1* in craniofacial development. Molecular mechanisms underlying the role of *Hic1* in craniofacial development remain largely unknown. Our objective was to elucidate the cellular fate of $Hic1^{+}$ cells during craniofacial development.

**Methods:** The fate of *Hic1*-expressing cells in craniofacial development was studied using lineage tracing analysis. A $Hic1^{CreERT2}$ mouse, in combination with a Cre-dependent reporter mouse, was used to label and follow *Hic1*-expressing cells. Reporter gene expression was induced at the onset of *Hic1* expression (embryonic age (E) of 10 days). Embryos were collected at E11.5, E13.5, E14.5, E16.5 and E18.5. The distribution and fate of reporter-expressing cells was determined using epi-fluorescence imaging. Micromass cultures of cells derived from the mandibular, frontonasal and maxillary prominences at E11.5 were used to study *Hic1*-expressing cells in cartilage formation. Samples (n=3) were fixed and stained with Alcian blue or COL2A1 to study the relationship of $Hic1^{+}$ cells to cartilaginous nodules. Single-cell RNA sequencing was performed on cells positive and negative for *Hic1*-expression in the head.

**Results:** *Hic1*$^{+}$ cells contribute to the mesenchyme within facial/masticatory muscles, tendon, tongue, meninges, nasal cartilage/ connective tissue, eyes, salivary gland stroma, teeth (dental papilla/pulp), and to populations of perineural and perivascular cells, including those within the brain. *Hic1* is not seen within the palatal shelves, or Meckel's cartilage. In micromass cultures of facial mesenchyme, most *Hic1*-expressing cells contribute to the area surrounding cartilaginous nodules, while few were incorporated within the nodules, mimicking the pattern of distribution of *Hic1*-expressing cells in the nasal structures. Single-cell RNA sequencing suggests *Hic1*-expressing cells are neural crest-like, and represent mesenchymal progenitors.

**Conclusions:** *Hic1*-expressing cells contribute to various mesenchymal tissues during craniofacial development, and likely represent a population of cranial neural crest-derived cells or similar.

## LAY SUMMARY

**Background:** This work focused on the tumour suppressor gene known as *Hypermethylated in cancer 1*, or *Hic1*, which is broadly expressed within embryonic mesenchymal tissues. When *Hic1* is deleted in mice, many craniofacial abnormalities result, including facial clefting and problems in the development of the skull, palate, eyes and ears.

**Objective:** Since the molecular mechanisms underlying the role of *Hic1* remain largely unknown, our objective was to understand the cellular fate of $Hic1^{+}$ cells during embryonic craniofacial development.

**Methods:** To reach this objective, we applied cellular methods that enable us to track cells expressing a gene of interest throughout development.

**Key results:** $Hic1^{+}$ cells and/or their progeny contribute to various mesenchymal tissues during craniofacial development, including facial and masticatory muscles, tendon, tongue, meninges, nasal cartilage and connective tissue, eyes, salivary gland stroma, teeth, and to populations of cells located around nerves and vessels, including those within the brain.

## PREFACE

- Dr. Underhill's laboratory previously identified the gene hypermethylated in cancer 1 (*Hic1*) in various murine embryonic tissues.
- Craniofacial-specific work included in this thesis, including the literature review, study design, cryosectioning, cell culture, staining, data analysis and writing was completed by Kathleen Martin, under the supervision of Dr. T. Michael Underhill.
- Mouse embryos were obtained, prepared and embedded by Wilder Scott, Martin Aróstegui, Daniel Taušan, Germain Ho and Kathleen Martin. Wilder Scott, Martin Aróstegui, Ryan Vander Werff and Tara Stach performed sample preparation for RNA single-cell sequencing. Andy Johnson and Justin Wong were involved in sorting cells for analysis at the UBC Flow Cytometry Facility.
- All animal work was approved by the UBC Animal Care Committee: Certificate #: A15-0202.
- This project was supported by the following Canadian Institutes of Health Research Grant: Mesenchymal progenitors and tissue regeneration PJT-14902 to Dr. T. Michael Underhill.
- The CIHR Frederick Banting and Charles Best Canada Graduate Scholarship - Master's Award to Kathleen Martin, provided further support.

# Table of Contents

**ABSTRACT** ..... **III**

**LAY SUMMARY** ..... **V**

**PREFACE** ..... **VI**

**LIST OF TABLES** ..... **IX**

**LIST OF FIGURES** ..... **X**

**LIST OF SYMBOLS** ..... **XI**

**LIST OF ABBREVIATIONS** ..... **XII**

**ACKNOWLEDGEMENTS** ..... **XIV**

**DEDICATION** ..... **XV**

**CHAPTER 1 - INTRODUCTION** ..... **1**

1.1 AN OVERVIEW OF CRANIOFACIAL DEVELOPMENT ..... 1

1.2 THE ROLE OF CRANIAL NEURAL CREST CELLS IN CRANIOFACIAL DEVELOPMENT ..... 6

1.3 NEUROCRISTOPATHIES ..... 9

1.4 THE CRANIAL, CARDIAC, VAGAL AND TRUNK NEURAL CREST SEGMENTS ..... 10

1.5 FATE MAPPING AND LINEAGE TRACING ANALYSIS OF NEURAL CREST CELLS ..... 11

1.6 INVOLVEMENT OF *HYPERMETHYLATED IN CANCER 1*$^{+}$ CELLS IN CRANIOFACIAL DEVELOPMENT ..... 16

1.7 OBJECTIVE AND AIMS ..... 19

**CHAPTER 2 – METHODS** ..... **20**

2.1 MOUSE MODEL ..... 20

*2.1.1 Tamoxifen* ..... *21*

*2.1.2 Mice* ..... *21*

*2.1.3 Collection of embryos* ..... *22*

2.2 CRYOPROCESSING ..... 22

*2.2.1 Staining of cryosections* ..... *23*

*2.2.2 Microscopy for fluorescent imaging* ..... *24*

*2.2.3. Structure identification* ..... *24*

2.3 MICROMASS CULTURES ..... 25

*2.3.1 Dissection for micromass cultures* ..... *25*

*2.3.2 Tissue processing for micromass cultures* ..... *26*

*2.3.3 Micromass cell culture* ..... *26*

*2.3.4 Staining of micromass cultures with Alcian blue* ..... *27*

*2.3.5 Staining of micromass cultures with COL2A1* ..... *28*

2.4 SINGLE-CELL RNA SEQUENCING OF *HIC1*$^{+}$ AND *HIC1*$^{-}$ CELLS OF THE HEAD ..... 28

*2.4.1 Hic1*$^{+}$ *and Hic1*$^{-}$ *cell isolation from the head* ..... *28*

**CHAPTER 3 – RESULTS** ..... **30**

3.1 DETERMINATION OF THE ONSET OF *HIC1* EXPRESSION IN EMBRYOS AT E8.5 AND E9.5 ..... 30

3.2 LINEAGE TRACING ANALYSIS OF *HIC1*-EXPRESSING CELLS ..... 32

3.3 IMMUNOFLUORESCENCE STAINING OF EMBRYOS FOR CD31, SOX9, AND NFH ..... 51

3.4 MICROMASS CULTURES ..... 58

3.5 SINGLE-CELL RNA SEQUENCING OF CELLS POSITIVE AND NEGATIVE FOR *HIC1*-EXPRESSION IN THE HEAD AT E11.5 ..... 61

**CHAPTER 4 – DISCUSSION** ..... **64**

4.1 LINEAGE TRACING ANALYSIS OF *HIC1*-EXPRESSING CELLS ..... 64
*4.1.1 Timing* ..... *64*
*4.1.2 Localization of the cellular fate of Hic1-expressing cells* ..... *64*
*4.1.3 A role for Hic1 in cleft palate* ..... *67*
*4.1.4 Hic1⁺ cells and tooth development* ..... *69*
4.2 *HIC1*⁺ CELLS AND CARTILAGE ..... 69
4.3 SINGLE-CELL RNA SEQUENCING ..... 71
4.4 CONCLUSION AND OVERALL SIGNIFICANCE ..... 72
4.5 STRENGTHS AND LIMITATIONS ..... 73
4.6 FUTURE DIRECTION ..... 76
**REFERENCES ..... 79**

## LIST OF TABLES

TABLE 1.1 CRANIOFACIAL DERIVATIVES OF CRANIAL NEURAL CREST CELLS…… 9

TABLE 2.1 LIST OF PRIMERS USED FOR GENOTYPING…… 22

TABLE 2.2 ANTIBODIES…… 24

## LIST OF FIGURES

FIGURE 1.1 MAMMALIAN CRANIOFACIAL DEVELOPMENT..... 2

FIGURE 2.1 TRANSGENIC MOUSE MODEL FOR LINEAGE TRACING ANALYSIS OF *HIC1*-EXPRESSING CELLS..... 21

FIGURE 3.1 LINEAGE TRACING ANALYSIS OF EMBRYOS WITH TAM ADMINISTERED AT E8.5..... 30

FIGURE 3.2 LINEAGE TRACING ANALYSIS OF EMBRYOS WITH TAM ADMINISTERED AT E9.5..... 31

FIGURE 3.3 LINEAGE TRACING ANALYSIS OF TRANSVERSE SECTIONS OF EMBRYOS AT E11.5..... 34

FIGURE 3.4 LINEAGE TRACING ANALYSIS OF TRANSVERSE SECTIONS OF EMBRYOS AT E13.5..... 35

FIGURE 3.5 LINEAGE TRACING ANALYSIS OF TRANSVERSE SECTIONS OF EMBRYOS AT E14.5..... 38

FIGURE 3.6 LINEAGE TRACING ANALYSIS OF TRANSVERSE SECTIONS OF EMBRYOS AT E16.5..... 40

FIGURE 3.7 LINEAGE TRACING ANALYSIS OF TRANSVERSE SECTIONS OF EMBRYOS AT E18.5..... 42

FIGURE 3.8 LINEAGE TRACING ANALYSIS OF CORONAL SECTIONS OF EMBRYOS AT E13.5, E14.5, E16.5, AND E18.5..... 45

FIGURE 3.9 LINEAGE TRACING ANALYSIS OF SAGITTAL SECTIONS OF EMBRYOS AT E11.5, E13.5, E14.5, E16.5 AND E18.5..... 48

FIGURE 3.10 LINEAGE TRACING ANALYSIS OF E20.5 EMBRYOS IN TRANSVERSE SECTIONS..... 50

FIGURE 3.11 SOX9 AND CD31 STAINING OF E13.5 EMBRYOS WITH TAM ADMINISTERED AT E9.5..... 52

FIGURE 3.12 EPI-FLUORESCENCE IMAGING OF ENDOTHELIAL CELL MARKER CD31 IN CORONAL SECTIONS OF E18.5 EMBRYOS..... 54

FIGURE 3.13 EPI-FLUORESCENCE IMAGING OF NEUROFILAMENT, A NEURON-SPECIFIC INTERMEDIATE FILAMENT..... 56

FIGURE 3.14 MICROMASS CULTURES OF THE COMBINED MAXILLARY, MANDIBULAR AND FRONTONASAL PROCESSES..... 59

FIGURE 3.15 SCRNA-SEQ PERFORMED ON *HIC1*$^{+}$ AND *HIC1*$^{-}$ CELLS DERIVED FROM THE HEAD..... 62

## LIST OF SYMBOLS

° degrees
α alpha
β beta
μm micrometer/ micron

**LIST OF ABBREVIATIONS**

Blast: basic local alignment search tool

BMP, BMP4: bone morphogenetic protein, bone morphogenetic protein 4

BSA: Bovine serum albumin

CD31: Cluster of differentiation 31

*Cd146*: *Cluster of differentiation 146*

CNCC: cranial neural crest cells

COL2A1: Type II collagen

*Des*: *Desmin*

DMEM: Dulbecco's Modified Eagle Medium

*Dmp1*: *Dentin matrix acidic phosphoprotein 1*

E: embryonic day

EC23: synthetic retinoid

EDTA: ethylenediaminetetraacetic acid

EGF: epidermal growth factor

*Eomes*: *Eomesodermin*

ET-1*:* endothelin-1

F-12: Ham's F-12 Nutrient Mix

FACS: fluorescence-activated cell sorting

FBS: fetal bovine serum

FGF*, Fgf8*: fibroblast growth factor, fibroblast growth factor 8

*Foxa2*: *Forkhead box A2*

*Hox*: homeobox

*LIS1, Lis1:* lissencephaly 1

MDS: Miller-Dieker syndrome

NCC: neural crest cells

NFH: neurofilament heavy chain

OCT: optimum cutting temperature formulation

PBS: phosphate buffered saline

PDGF: platelet-derived growth factor

PFA: paraformaldehyde

PSA: Puck's saline A

TAM: tamoxifen

TCOF1, *Tcof1*: *Treacle ribosome biogenesis factor 1*

tdTomato: tandem dimer Tomato

TGFα: transforming growth factor α

TGFβ: transforming growth factor β

scRNA-seq: single-cell RNA sequencing

SHH: Sonic Hedgehog

SOX9, *Sox9*: *SRY-box 9*

*Sox10*: *SRY-box 10*

*Wnt*: *Wingless*

*Wnt1: Wingless-type MMTV integration factor site family member 1*

*Wnt3a*: *Wingless-type MMTV integration factor site family member 3a*

**ACKNOWLEDGEMENTS**

First and foremost, I would like to thank my supervisor Dr. Michael Underhill. Your guidance and mentorship in completing this project were invaluable.

Secondly, I wouldn't have made it through these past 10 years of university without my friends and family. Mom, Dad and Marianne- I would like to thank you for the endless support and encouragement. Aunt Elizabeth- your saying "stick with science" clearly stuck. Thank you for instilling an appreciation for science in me. Fabian- thank you for your patience and positivity these past few months. The light at the end of the tunnel is near.

This work would not have been possible without the assistance and hard work of past and present members of the Underhill Lab: Wilder Scott, Martin Aróstegui, Dr. Lauren Martin, Dr. Kim Wiegand, Germain Ho, Daniel Taušan, George Gordon Davenport III, Amanda Yang, and Cindy Crichlow. Thank you.

To my committee members: Dr. Edward Putnins and Dr. Timothy O'Connor: Thank you for your help and input with this project.

Finally, I would like to thank my orthodontic co-residents, Negar, Rob and Suliman for making the last three years enjoyable ones. You truly were a pleasure to work with, and to that, I extend my thanks.

**DEDICATION**

*To my family*

# CHAPTER 1 - INTRODUCTION

## 1.1 An overview of craniofacial development

Craniofacial development occurs by means of concerted interactions between different cell types and tissues, in particular locations, at specific times. Mammalian facial development is evident around 4 weeks in humans and 8.25 days (E8.25) in mice, with the appearance of the first branchial arch (Trumpp et al., 1999) (Diewert, 1985). In embryonic development, the these bud-like branchial arches are composed of undifferentiated mesenchyme with a mesodermal core and an outer covering of epithelium (Trumpp et al., 1999). The first branchial arch gives rise to the mandibular and maxillary arches that later become the maxilla and the mandible. In mice, the first and second branchial arches and the frontonasal prominence can be seen around E9.5 days, and by E10.5 days, five facial prominences appear, forming around the stomatodeum, or primitive mouth (Chai et al., 2000). These include one frontonasal prominence superiorly, two maxillary processes laterally, and two mandibular processes inferiorly (Bush and Jiang, 2012). The frontonasal process will contribute to the nose and the upper lip; the two maxillary processes will form the maxilla, a part of the upper lip and the secondary palate; the two mandibular processes will give rise to the mandible and part of the tongue (Huang and Thesleff, 2013). A figure demonstrating these various embryonic structures in craniofacial development is shown below (Figure 1.1). Cranial neural crest cells (CNCCs) which originate from the dorsal folds overlying the developing neural tube, contribute to these five facial prominences (Bush and Jiang, 2012). Around day 41 in humans and E12 in mice, the frontonasal prominence produces a medial and a lateral nasal process on both the left and right sides, with the nasal pits, or future nostrils, located between the two processes (Bush and Jiang, 2012) (Wilkie and Morriss-Kay,

2001). Together, the lateral and medial nasal processes will form the nostrils and nose, and the medial nasal process, along with the maxillary process, will form the upper lip (Bush and Jiang, 2012). The development of the first branchial arch is critical in craniofacial development. Over one hundred and thirty human syndromes demonstrate problems in the formation of the first branchial arch (Trumpp et al., 1999).

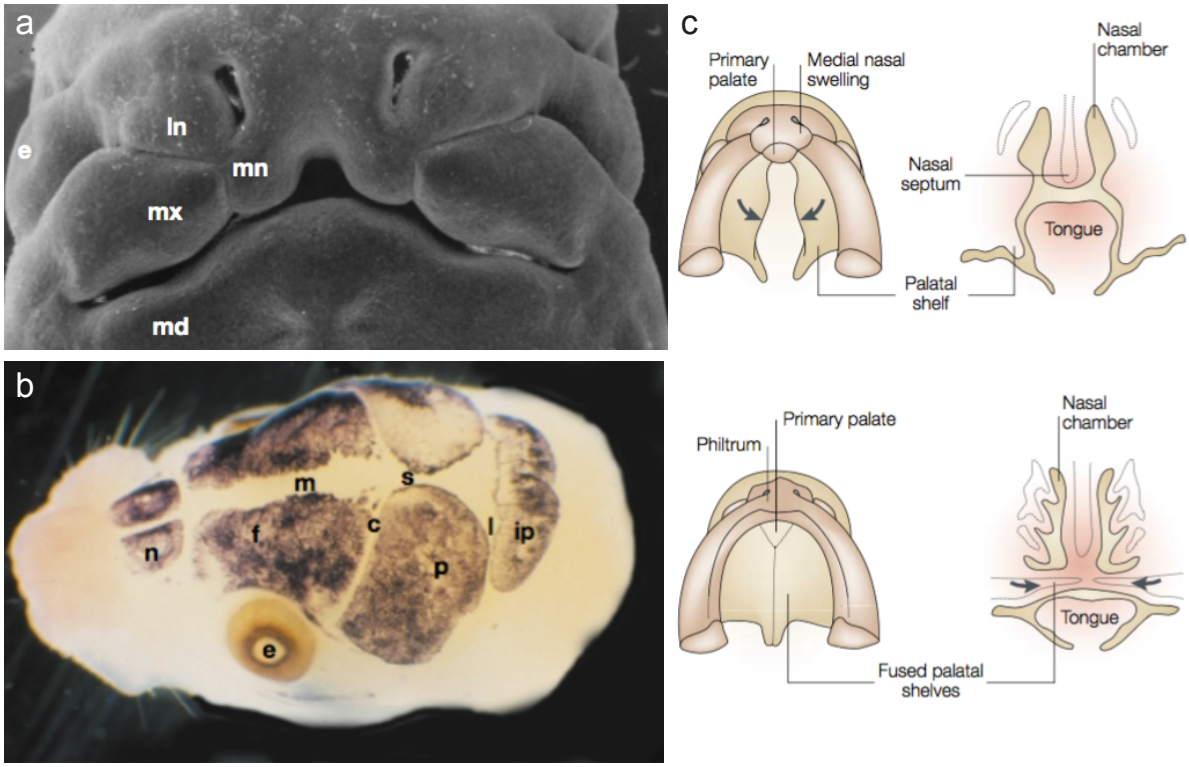


**Figure 1.1 Mammalian craniofacial development (adapted from Wilkie and Morriss-Kay, 2001)**

**(a)** The facial processes form surrounding the developing mouth, at around 41 days and E12.0 days in human and mouse embryonic development, respectively. These processes are composed of neural crest-derived mesenchyme, and they include the two maxillary (mx), two mandibular (mn), two lateral nasal (ln) and two medial nasal (mn) processes. The mandibular and maxillary processes give rise to the mandible and maxilla, both of which are derivatives

of the first branchial arch. Together, the medial nasal and maxillary processes join to form the upper lip, and the two medial nasal processes unite to form the philtrum of the upper lip, the upper incisors and the primary palate in which these teeth reside. The lateral nasal processes form the alae of the nose. e=eye. (**b)** A mouse head at E16 days (approximately 4 months in humans) demonstrates ossification of the bones of the skull vault, and the interposed cranial sutures. f=frontal bone, ip= interparietal bone, n=nasal bone, p=parietal bone, c=coronal suture, l=lambdoid suture, m=metopic suture, s=sagittal suture, e=eye. (**c)** From weeks 7-10 in humans, and E12.5-14.5/15.5 in mice, the formation of the secondary palate occurs. The right and left maxillary processes give rise to palatal shelves that contribute to the formation of the secondary palate. In order for the secondary palate to form, these two palatal shelves must unite with one another (arrows), and with the nasal septum. To unite, the palatal shelves must not only grow in size, but must also re-orient from a vertical position on either side of the tongue, to a horizontal position, as the tongue descends.

Facial prominences must unite by one of two processes: fusion or merging (Cox, 2004). In merging, separated outgrowths "fill in" the groove between the prominences by means of mesenchymal proliferation and cellular migration, and this is the method by which the maxillary process unites with the lateral nasal process, the mandibular processes join together, and the maxillary and mandibular processes partially unite (Cox, 2004). Fusion, on the other hand, involves the meeting of two separate outgrowths, with apoptosis and cellular changes occurring in the epithelial edges that meet (Cox, 2004). Fusion occurs in the union of the maxillary processes in the formation of the secondary palate, in the joining of the medial nasal processes with each other in the formation of the primary palate and philtrum of

the upper lip, and between the maxillary and medial nasal processes in the formation of the upper lip (Cox, 2004).

The palate separates the oral cavity from the overlying nasal cavity, and consists of a bony hard palate anteriorly, and a muscular soft palate posteriorly. Anteriorly, the hard palate is comprised of the primary and the secondary palate. The smaller of the two, the primary palate, forms from the fusion of the two mesial nasal processes around day 41 in humans and E12 days in mice (Wilkie and Morriss-Kay, 2001). The primary palate is positioned in front of the incisive foramen and contains the four maxillary incisors. Posterior to the incisive foramen lies the secondary palate. Development of the secondary palate occurs from weeks 7-10 in humans and from E12.5 to approximately E14.5/15.5 in mice, as bilateral outgrowths of the maxillary processes (Ferguson, 1988) (Wilkie and Morriss-Kay, 2001). In mammals, the growth of these palatal shelves initially occurs in a vertical direction, alongside the lateral aspect of the tongue (Ferguson, 1988). Eventually, however, as the mandible grows in length and the tongue descends, the palatal shelves become orientated horizontally above the dorsal surface of the tongue, allowing for the shelves to meet and fusion to occur, thereby establishing a continuous palate (Ferguson, 1988) (Huang and Thesleff, 2013). During fusion, the shelves adhere and the mesial edge epithelium of each shelf creates a midline epithelial seam that is removed via cell death, cell migration and an epithelial-mesenchymal transition (Ferguson, 1988) (Hilliard et al., 2005). Interruption of any process of palatal development may lead to the development of cleft palate. These disruptions may include disturbances in the growth of the palatal shelves, a delay in or failure of the palatal shelves to elevate to a horizontal position above the tongue, problems in fusion of the palatal shelves,

the inability to remove the midline epithelial seam, rupture following palatal fusion, or a failure of the palatal mesenchyme to differentiate (Ferguson, 1988).

The skull is formed from twenty-two individual bones which can be categorized into two groups: the neurocranium and the viscerocranium (Wilkie and Morriss-Kay, 2001). The frontal, sphenoid, occipital and paired temporal and parietal bones constitute the skull vault of the neurocranium, and serve to protect the brain and sensory organs, while the mandible, and paired maxillae, zygomatic bones, nasal bones, palatine bones, and auditory bones (malleus, incus, stapes) form the viscerocranium (Wilkie and Morriss-Kay, 2001). The viscerocranium is comprised entirely of CNCCs, and the neurocranium is made from both mesodermal and CNCC sources (Jiang et al., 2002). The neurocranium consists of the intramembranous skull vault and the cartilaginous cranial base (McBratney-Owen et al., 2008). In mice, the CNCC-derived cranial base cartilages include the trabecular, paranasal, frontal, orbital, hypophyseal and pterygoid cartilages of the anterior cranial base (McBratney-Owen et al., 2008). The hypochiasmatic cartilages are mesodermal in nature, and also help form the anterior cranial base (McBratney-Owen et al., 2008). The posterior cranial base is entirely mesodermally-derived, and is formed from the following cartilages: auditory capsules, parachordal, acrochordal, exoccipital, and supraoccipital (McBratney-Owen et al., 2008). In mice, the cranial base initiates chondrogenesis around E11 and is completely formed by E16 (McBratney-Owen et al., 2008). The cranial base extends from the nasal septum, anteriorly, to the foramen magnum, posteriorly, and its development is important for proper formation of the cranial vault and viscerocranium (McBratney-Owen et al., 2008).

Meckel's cartilage develops in the mandibular arch from an aggregation of ectomesenchymal cells, around the area of the future molars (Chai et al., 2000). This

cartilage elongates in an anterior-posterior direction, forming a template for the development of the mandible, in addition to the future middle ear bones, the malleus and incus (Chai et al., 1994).

The mouse is the ideal model organism for studying human craniofacial development, because the development of the mouse head accurately represents the development of the human head (Wilkie and Morriss-Kay, 2001). Other model organisms, such as avian, fish and amphibian models do not reflect human head development as closely (Wilkie and Morriss-Kay, 2001). For example, these species do not have a comparable bony palate or cranial sutures (Wilkie and Morriss-Kay, 2001).

## 1.2 The role of cranial neural crest cells in craniofacial development

The population of cells that significantly contributes the branchial arches and facial primordia during craniofacial embryonic development is known as the CNCCs. Neural crest cells (NCCs) represent a specific population of cells that is multipotent, unique to vertebrates, and critical in the formation of many craniofacial structures (Huang and Thesleff, 2013). NCCs are often coined "the fourth germ layer," because they gives rise to neural and mesenchymal cell types that typically arise from the ectoderm or the mesoderm (Dupin et al., 2018) (Hall, 2000). In order to form NCC-derived tissues, the population of NCCs first needs to be established. The neural crest originates from neuroectodermal tissue located at the lateral ridges or "crests" of the closing neural folds, which elevate 20 days following conception in humans (Sperber et al., 2010) (Achilleos and Trainor, 2012). An epithelial-mesenchymal transition (EMT) occurs within the population of NCCs, at the dorsal aspect of the neural tube, allowing for these cells to delaminate (Ahlstrom and Erickson, 2009) (Achilleos and Trainor, 2012). This process is similar to the previously mentioned EMT that

happens at the midline epithelial seam of the palate. Next, migration of the NCCs ensues. These cells, which have substantial migratory capabilities, begin to stream ventrolaterally, around 21 days in humans and around the 4-somite stage (~8 days) in mice (Sperber et al., 2010) (Huang and Thesleff, 2013) (Nichols, 1981). It has been noted that the migration of CNCCs is similar between the mouse and the human (O'Rahilly and Müller, 2007). Finally, the NCCs will invade tissues, reach their final destination and differentiate, contributing to a diverse array of cell types, as demonstrated in Table 1, which outlines the derivatives of CNCCs.

The cellular types that the NCCs will form are both genetically pre-determined and environmentally influenced (Sperber et al., 2010). These NCCs may have predetermined fates as they migrate into the branchial arches, or they may have their identity determined later on, within the destined tissue. Various signaling pathways and factors regulate the fate, location and patterning of the CNCCs, including but not limited to: endothelin-1 (ET-1), fibroblast growth factor (FGF), transforming growth factor β (TGFβ), wingless (Wnt), platelet-derived growth factor (PDGF), bone morphogenic protein (BMP), sonic hedgehog (SHH), retinoic acid, epidermal growth factor (EGF), and transforming growth factor alpha (TGFα) (Minoux and Rijli, 2010) (Francis-West et al., 1998). These signals may not come directly from the NCCs, but may be from adjacent tissues and cells, adding to the complexity of development. For example, when fibroblast growth factor 8 (*Fgf8*) is inactivated in surface ectoderm, the CNCC-derived ectomesenchyme is affected, leading to problems in in cell survival, morphogenesis, patterning and outgrowth within the first branchial arch (Trumpp et al., 1999). This demonstrates the importance of signalling from the ectoderm to the developing mesenchyme in facial development. With respect to NCC proliferation, when

*Wnt1* and *Wnt3a* are mutated together, a deficiency in tissues derived from NCCs results, suggesting that these genes are needed for the expansion of dorsal neural precursors (Ikeya et al., 1997). Also, the development of the cranial ganglia, which are derived from CNCC, is disturbed by the mutation of *SRY-box 10 (Sox10),* and *Sox10* may play a role in specifying the regional identity of the CNCCs (Herbarth et al., 1998). Key players in the regulation of the patterning of the CNCCs within the branchial arches are the distal-less homeobox genes (Huang and Thesleff, 2013). Retinoic acid signalling is also involved in patterning, particularly in the frontonasal prominence and its derivatives (Minoux and Rijli, 2010).

**Table 1.1 Craniofacial derivatives of cranial neural crest cells**

(Sperber *et al*., 2010), (Ito et al., 2003) (Chai et al., 2000) (Dupin et al., 2018), (Creuzet et al., 2002) (Wilkie and Morriss-Kay, 2001)

| |
|---|
| **Nervous-system related:**<br>-Supporting tissues: Schwann cells, glial cells, meninges (pia mater, arachnoid mater, dura mater)<br>-Sensory ganglia: sensory ganglia and nerves (i.e. trigeminal, facial, glossopharyngeal and vagal), spinal dorsal root ganglia<br>-Autonomic nervous system: sympathetic ganglia and plexuses, parasympathetic ganglia (ciliary, ethmoid, sphenopalatine, submandibular) |
| **Skin-related:** Melanocytes, dermis of the skin of the face and ventral neck |
| **Skeletal:** *Ectomesenchyme of the facial prominences/pharyngeal arches*<br>-Bones: squamosal, frontal, basisphenoid, maxilla, mandible, auditory ossicles, zygoma, nasal (*The entire viscerocranium, select bones of the neurocranium* i.e. CNCCs do not contribute to the parietal bone, basioccipital bone, non-squamous temporal bone)<br>-Cartilages: multiple skull (basisphenoid, ethmoid, presphenoid) and pharyngeal arch cartilages (i.e. Meckel's cartilage), hyoid cartilage, nasal capsule<br>-Cells: Chondrocytes and bone cells<br>-Tendon |
| **Muscular:** ciliary muscles of the eye, dermal smooth muscle of the skin, vascular smooth muscles, connective tissue elements of the pharyngeal arch muscles including those of the facial, and masticatory muscles (in combination with mesodermal elements) |
| **Vascular:** blood vessel wall-associated cell types excluding the endothelium |
| **Other connective tissues:** adipocytes |
| **Glandular**: stroma of the salivary, pituitary and lacrimal glands |
| **Eye:** cornea and sclera of the eye, melanophores of the iris |
| **Dental:** dentin and pulp of the teeth, odontoblasts, alveolar bone, periodontal ligament |

## 1.3 Neurocristopathies

As the NCCs migrate, they also divide, increasing the size of the migratory population. Abnormalities in NCC proliferation and migration can lead to conditions called neurocristopathies (O'Rahilly and Müller, 2007). Treacher Collins syndrome (OMIM # 154500) is an example of a neurocristopathy in which there is a decreased number of migrating NCCs, and a reduction in the proliferative capacity of these cells (Dixon et al.,

2007). Haploinufficiency of *Tcof1* in mice has been found to result in apoptosis of NCC precursors, thereby reducing the number of cells that can populate the first and second branchial arches during development (Dixon et al., 2007). Clinically in humans, this autosomal dominant disorder, resulting from the loss-of-function mutation of the gene TCOF1, presents with abnormalities in first and second branchial arch structures derived from CNCCs (Dixon et al., 2007). These include a spectrum of features, some of the most common being: mandibular retrognathia, hypoplasia or absence of the zygoma, external ear abnormalities, conductive hearing loss due to malformed auditory ossicles, airway compromise, downward sloping of the palpebral fissures with colobomas (notches) of the lower eyelid and a lack of eyelashes medial to the notch, as well as cleft palate (Dixon et al., 2007). Treacher Collins syndrome exemplifies the significance of CNCC populations in craniofacial development, and demonstrates the importance of unraveling the molecular basis of craniofacial anomalies to better understand the variable clinical appearances and improve the management of these conditions.

### 1.4 The cranial, cardiac, vagal and trunk neural crest segments

The cells of the neural crest are thought to originate from four distinct segments of the neural axis (Achilleos and Trainor, 2012). Specifically, these are the cranial, cardiac, vagal and trunk NCCs. The cranial neural crest gives rise to the most diverse types of cells (Table 1), compared to the other three segments, including a significant proportion of the craniofacial bone and cartilage (Achilleos and Trainor, 2012). The head is the only part of the body with skeletal elements that are identified as NCC derivatives (Wilkie and Morriss-Kay, 2001). In the remainder of the body, bone and cartilage are derived from the mesoderm (Dupin et al., 2018). The cardiac neural crest (NC) forms the aorticopulmonary septum and conotruncal

cushions of the heart, while the vagal NC contributes to the enteric ganglia (Achilleos and Trainor, 2012). The trunk NC forms neurons and glia, the peripheral nervous system, adrenomedullary cells and melanocytes (Le Douarin, 1999). Although the trunk NCCs appear to have more restricted cellular fates, work has demonstrated that these cells demonstrate the capacity for mesenchymal differentiation *in vitro* (Dupin et al., 2018) (John et al., 2011) (Ido and Ito, 2006).

The environment surrounding these two populations may be important in regulating cellular fate. For example, homeobox (*Hox)* gene expression, which is important in patterning, is absent from where the head skeleton develops, and is present elsewhere in the body (Dupin et al., 2018) (Couly et al., 1998). Furthermore, ectopic *Hox* gene expression can actually prevent the development of the head skeleton (Creuzet et al., 2002). By comparing the genetic profiles of trunk and CNCCs and improving our understanding of the different environmental cues these two cellular populations receive, we may gain insight into why a NCC will differentiate into a certain cell type.

## 1.5 Fate mapping and lineage tracing analysis of neural crest cells

In order to determine whether or not a NCC is multipotent or if the fate of the cell is pre-determined before migration, a chick chimera model was employed. In a chick embryo, an area of the trunk neural tube was ablated before NCC migration began (Le Douarin et al., 1975). This region would normally give rise to cholinergic neurons (Le Douarin et al., 1975). It was replaced with a different trunk region from a quail at the same developmental stage (Le Douarin et al., 1975). Normally, this trunk region from the quail gave rise to adrenergic neurons (Le Douarin et al., 1975). When grafted, the adrenergic precursors from the quail could generate cholinergic neurons in the chick (Le Douarin et al., 1975). This confirmed that

the cellular fate and plasticity of the NCCs was not fully determined prior to migration, and depended on the environment (Achilleos and Trainor, 2012). Subsequent studies determined that a premigratory quail trunk NCC could differentiate into both melanocytes and neuronal cells, confirming the multipotency of these cells (Cohen, 1977). Later, vital dyes served as a method to mark NCCs and track them throughout their migration. Not only were the premigratory NCCs multipotent, but so too were the migratory NCCs (Achilleos and Trainor, 2012). An example of a vital dye is the fluorescent dye DiI, employed by Serbedzija in order to trace the lineage of premigratory NCCs (Serbedzija et al., 1989). In the grafting experiments, difficulties in microsurgery and culturing of embryos posed challenges (Chai et al., 2000). In the vital dye studies, it was uncertain whether all NCCs were labelled and whether non-specific labeling occurred (Chai et al., 2000). Furthermore, it was challenging to maintain the dye throughout the entire embryonic developmental period (Chai et al., 2000). Another method for lineage tracing analysis involved the administration of a *LacZ*-containing retrovirus into migrating NCCs (Poelmann and Gittenberger-de Groot, 1999). A weakness here, however, was that this method may not label all of the migrating NCCs.

In order to overcome the limitations of tissue transplantation, vital dye labeling, and viral infection, the *Wnt1-Cre/ R26R* model was created as a method of indelibly marking the NCC line by causing CNCCs to express *LacZ* (Chai et al., 2000). For this model, Chai *et al* applied a transgenic mouse system in order to determine the fate of CNCCs in the development of the mandible and the teeth from E9.5-6 weeks (Chai et al., 2000). This genetic system was composed of two mouse lines. In one line, Cre recombinase expression was controlled by the promoter of the *Wnt1* transgene (*Wnt1*-Cre mouse), and in the other line, Cre-mediated recombination allowed for the expression of the ROSA26 conditional

reporter (Chai et al., 2000). This reporter showed β-galactosidase expression in all cells in which the Cre was activated (Soriano, 1999). Expression of the proto-oncogene *Wnt1* is limited to a population of migrating NCCs, making it a suitable transgene for following CNCC migration and differentiation (Chai et al., 2000). Here, the CNCCs and their progeny were indelibly marked, and were seen to give rise to nerve ganglia of the branchial arches, the articular disc of the temporomandibular joint, chondrocytes in Meckel's cartilage, the palatine bone and its periosteum and various dental structures (Chai et al., 2000). Specifically, these dental structures included the condensed dental mesenchyme, the dental papilla, odontoblasts, dentine matrix, pulp, cementum and periodontal ligament (Chai et al., 2000). With regards to timing, at E9.5, the *Wnt1-Cre/R26R* mice demonstrated *Wnt1*-labelled-CNCCs and progeny in the frontonasal prominence, the first and second branchial arches, the spinal dorsal root ganglia, and the trigeminal and facial nerve ganglia (Chai et al., 2000). At E10.5, *Wnt1*-expressing cells and progeny were present in frontonasal prominence around the nasal pit, the maxillary and mandibular prominences, the ganglia of the trigeminal nerve, facial nerve, glossopharyngeal nerve and vagus nerve, as well as in the second and third branchial arches (Chai et al., 2000). Migration of the CNCCs was seen at E10.5, in a ventrolateral direction, subectodermally, into the first branchial arch, as would be expected for a CNCC population (Chai et al., 2000). The $Wnt1^{+}$ cells and their progeny were closely associated with the ectoderm, but did not contribute to the ectoderm, as is also consistent with NCCs (Chai et al., 2000). In another study, the *Wnt1-Cre/R26R* model demonstrated that a significant majority of the mesenchyme contained in the palate is of CNCC-origin, with the remainder being mesodermally derived (Ito et al., 2003). Furthermore, this model has shown that the dura

mater is CNCC-derived and that the dura is required for proper skull formation (Ito et al., 2003).

This two-component genetic system allowed for CNCCs to be followed during craniofacial development, and this served as a method for comprehensively analyzing cellular fate. A weakness in this system is that detection of β-galactosidase (*LacZ*) activity depends on staining, and the literature mentions incomplete penetration in the serially sectioned samples (Chai et al., 2000). In this study, the *Wnt1* expressing cells were specific to CNCCs, and the authors claimed that the R26R-reporter demonstrated good specificity and did not demonstrate ectopic expression (Chai et al., 2000). In 2013, Lewis *et al* detected ectopic transgene expression in this *Wnt1-Cre* transgenic mouse line that was resulting in the activation of Wnt signaling and leading to changes in midbrain development, including midbrain enlargement (Lewis et al., 2013). These phenotypic changes complicate the applications of this mouse line in developmental research. This discovery of ectopic expression of *Wnt1* from the *Wnt1-Cre* transgene led to the creation of a new *Wnt1-Cre2* transgenic mouse line, which did not exhibit the ectopic transgene expression (Lewis et al., 2013).

Interestingly, non-CNCC-derived mesenchymal cells were present within the branchial arches, along with the *Wnt1*-labelled-CNCC-derived cells (Chai et al., 2000). This was especially evident within Meckel's cartilage (Chai et al., 2000). The authors concluded that either the $Wnt1^{-}$ cells in Meckel's cartilage were from ventrally emigrating neural tube cells, or that the *Wnt1*-expressing cells may only represent a subpopulation of CNCCs that contribute to craniofacial structures (Chai et al., 2000). If the latter is true, than it is possible that specific subpopulations of NCCs give rise to specific NCC-derivatives. If this is the case,

then further identification and fate mapping of NCC derivatives using novel markers for CNCCs may help us to improve our understanding of the cellular origins of mesenchymal derivatives, and the signaling pathways affecting NCC migration and differentiation. The gene, *Hypermethylated in cancer 1* (*Hic1*), discussed in the section below, may represent a novel marker for understanding the development of the craniofacial mesenchyme.

Finally, it is important to mention the *in vivo* fate mapping study conducted by Baggiolini *et al* that sought to determine whether NCCs are multipotent or simply composed of a variety of cells with pre-determined/ lineage-restricted fates (Baggioloni et al., 2015). This study applied the *R26R-Confetti* mouse model that allows different clones to be identified within the same specimen (Baggioloni et al., 2015). The *R26R-Confetti* model does not require cellular isolation, transplantation or removal of cells from their native microenvironment, that is advantageous as these procedures can induce a "stemness" program (Baggioloni et al., 2015) (Snippert and Clevers, 2011). For cellular fate mapping of the premigratory NCCs and migratory NCCs, the *Wnt1-CreER*$^{T}$ and *Sox10-CreER*$^{T2}$ mouse lines were used, respectively (Baggioloni et al., 2015). *Sox10* expression occurs after *Wnt1* expression and labels nearly all NCCs once they delaminate from the dorsal neural tube (Baggioloni et al., 2015) (Hari et al., 2012). In both the premigratory and migratory NCC populations studied, the majority of NCCs were found to be multipotent, and only a few clones gave rise to single derivatives. The trunk NCCs in this study contributed to many structures, including the dorsal root ganglia, Schwann cells, and cells that generate melanocytes, in both the premigratory and migratory populations. Most of the NCCs in this study were multipotent, but within each clone the composition of cell types was variable. For example, some of the multipotent clones produced all possible fates while other clones were

restricted and only produced two types of cells. This study provides us with evidence for the multipotent nature of both premigratory and migratory trunk NCCs. Here, *Wnt1* and *Sox10* served as useful markers in studying the premigratory and migratory population of NCCs within the trunk.

## 1.6 Involvement of *Hypermethylated in cancer 1*$^{+}$ cells in craniofacial development

Previous work in the Underhill Lab has found *Hic1* to be broadly expressed within murine embryonic mesenchymal tissues, suggesting a role for *Hic1* in development. *HIC1* is a candidate tumour suppressor gene that resides at 17p13.3 and encodes for the zinc-finger transcription factor HIC1 (Wales et al., 1995). It was found that in normal tissues, *HIC1* is ubiquitously expressed, while in cancerous tissue, it is frequently hypermethylated and under-expressed (Wales et al., 1995). A basic local alignment search tool (Blast) was performed in order to compare the homology of the gene sequences between the mouse, and the chicken and human. When compared with the murine sequence for *Hic1*, chicken showed 68.3% of orthologous sequence matching, and human showed 94.8% orthologous matching (Ensembl genome browser 92). A Blast was also performed to assess protein homology. This demonstrated 95% identity between mouse and human, and 63% identity between mouse and chicken (National Center for Biotechnology Information, U.S. National Library of Medicine). The homology between the mouse and human is high at both the protein and gene levels.

In 2000, Carter *et al* generated and analyzed the *Hic1* knockout mouse. Of all the 20 knockouts generated, no homozygous knockout mice survived past E18.5, which implies the *Hic1*$^{-/-}$ condition is embryonic lethal (Carter et al., 2000). Analysis of *Hic1*$^{-/-}$ knockout embryos from E11.5-E18.5 demonstrated a great variety of abnormalities, while *Hic1*$^{+/-}$ and *Hic1*$^{+/+}$ embryos did not demonstrate these developmental defects, which included gross

underdevelopment and smaller overall size, a pale appearance, ventral body defects, limb and digit dysmorphology, and multiple craniofacial anomalies, all of which are of particular interest to this study (Carter et al., 2000). The craniofacial anomalies seen included: facial clefting, a lack of fusion between the maxillary processes and mandibular arches, abnormal closure/ truncation of the secondary palate, low-set/ underdeveloped ears, abnormal eye development including missing eyes or a fused eyespot, holoprosencephaly (or failure of forebrain to develop into two hemispheres), shortened snouts, the absence of dura mater that gives rise to the cranial bones, acrania (the partial or complete absence of the bones of the cranial vault), and exencephaly (the protrusion of the brain outside of the skull) (Carter et al., 2000). This suggests a role for *Hic1* in craniofacial development. Interestingly, holoprosencephaly, which consists of the single fused eyespot and the protrusion of the telencephalon, as well as the failure of fusion of the maxillary and mandibular processes at the midline, is a characteristic phenotype of *Shh*-deficiency (Chiang et al., 1996). It should be noted that there was substantial phenotypic variation in the appearance of these *Hic1* knockouts, with embryos differing greatly in the features presented (Carter et al., 2000).

The features seen in the *Hic1* knockout mouse are similar to those exhibited in Miller-Dieker Syndrome (MDS) (OMIM # 247200), that include a prominent forehead, brachycephaly, a long and thickened upper lip, bitemporal narrowing, hypertelorism, up-slanting of the palpebral fissures, a shortened/ upturned nose with a low nasal bridge, flat ears, a flat midface, and small chin in addition to limb/digit defects and omphalocele (protrusion of abdominal organs outside of the body) (Carter et al., 2000) (Allanson et al., 1998). MDS also involves lissencephaly, a malformation of the brain in which the cerebrum has a smooth surface, resulting from a migratory delay or an arrest of neurons, as well as

intellectual disability (Allanson et al., 1998). The gene lissencephaly 1 (*LIS1)* which is mutated in cases of lissencephaly is located on 17p13.3, within the 350kB region affected in MDS, as is *HIC1* (Carter et al., 2000). Although MDS patients are affected with lissencephaly, this feature was not evident in the *Hic1* knockouts, though it was in mice with decreased *Lis1* activity (Hirotsune et al., 1998).

## 1.7 Objective and aims

**Objective:** Since the molecular mechanisms underlying the role of *Hic1* in craniofacial development remain largely unknown, our objective was to elucidate the cellular fate of $Hic1^{+}$ cells during embryonic craniofacial development.

**Hypothesis:** Our hypothesis was that *Hic1* is expressed by a population of mesenchymal progenitor cells of NCC origin or similar that contribute to the prenatal development of craniofacial mesenchymal tissues.

**The specific aims of this study are:**

**Aim 1:** To study the fate of *Hic1*-expressing cells in craniofacial development using lineage tracing analysis.

A $Hic1^{CreERT2}$ mouse, in combination with a Cre-dependent reporter mouse, would be used to label and follow *Hic1*-expressing cells. Reporter gene expression would be induced at the onset of *Hic1* expression. The distribution and fate of reporter-expressing cells would be determined using epi-fluorescence imaging.

**Aim 2:** To study the involvement of $Hic1^{+}$ cells in cartilage formation, using micromass cultures of cells derived from the mandibular, frontonasal and maxillary prominences.

**Aim 3:** To characterize $Hic1^{+}$ cells in craniofacial development by performing single-cell RNA sequencing (scRNA-seq) in order to compare gene expression of cells positive and negative for *Hic1*-expression in the developing head.

# CHAPTER 2 – METHODS

## 2.1 Mouse model

A *Hic1*$^{CreERT2}$ mouse was crossed with a Cre-dependent tandem dimer Tomato (tdTomato)-based reporter mouse, in which tdTomato expression was dependent upon removal of the LoxP-flanked stop cassette upstream of the tdTomato gene (Rosa26-CAG-loxP-stop-loxP-tdTomato) (Figure 2.1). *Hic1*$^{CreERT2}$ mice were generated by genOway Inc, and the tdTomato-based reporter mice, Rosa-tdTomato$^{f/+}$, were acquired from Jackson Laboratory (B6.Cg-Gt(ROSA)26Sortm$^{14(CAG-tdTomato)Hze}$/J (Jax stock number 007914). The Cre in the CreERT2 was fused to a modified estrogen receptor with increased affinity for TAM. In the absence of TAM, the CreERT2 accumulates in the cytoplasm. Following addition of TAM the CreERT2 fusion protein could enter the nucleus and remove the LoxP-flanked stop cassette (Jaisser, 2000). It should be noted that the floxed transcriptional stop cassette consists of three strong polyadenylation signals in tandem upstream of the tdTomato reporter. This prevents the tdTomato protein from being expressed in the absence of Cre-mediated deletion of the floxed stop cassette. In this system, when TAM was administered to the pregnant dam via oral gavage, *Hic1*$^{+}$ cells began to express the tdTomato fluorescent protein permanently. Any progeny of the *Hic1*$^{+}$ cells also expressed the tdTomato fluorescent protein. This enabled us to map the fate of *Hic1*$^{+}$ cells and their progeny throughout development.

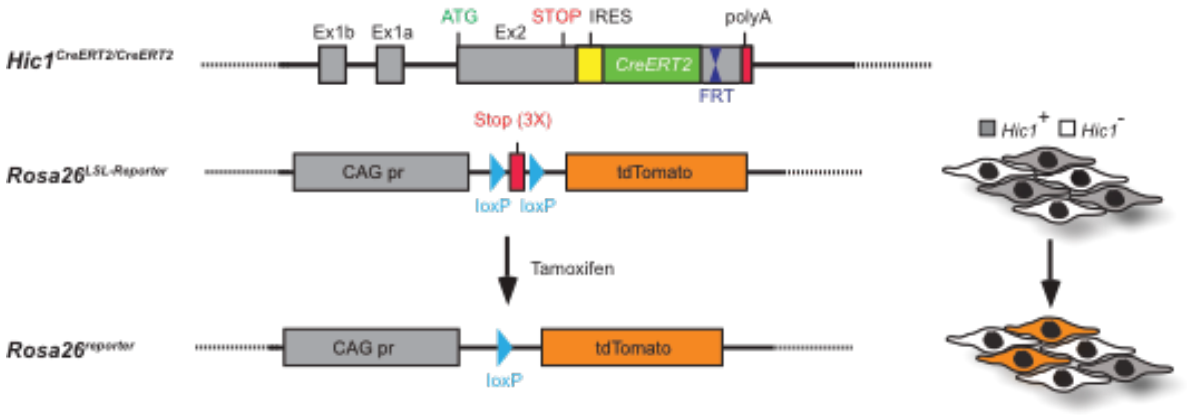


**Figure 2.1 Transgenic mouse model for lineage tracing analysis of *Hic1*-expressing cells.**

### 2.1.1 Tamoxifen

Tamoxifen (TAM) (Sigma-Aldrich T5648) stock solution was prepared weekly at a concentration of 25mg/mL in corn oil (Sigma C8267), and stored at 4°C. Before administration, stock was rewarmed at 37°C in a rotating chamber. Pregnant dams were given TAM via oral gavage at 2mg/20g mouse using a 300uL dose in order to induce reporter gene expression. The effectiveness of TAM to induce Cre activation in the embryo is typically restricted to ~ 12 hrs (Nakamura et al., 2006).

### 2.1.2 Mice

C57B1/6 mice were used in this experiment. Mice were raised in groups with a 12-hour light-dark cycle, and were fed *ad libitum* with laboratory chow and water. Genotyping was performed using DNA obtained from ear punches taken when mice were 3-8 weeks old. The UBC Genotyping Facility isolated DNA and performed the mice genotyping via polymerase chain reaction amplicon analysis. The following primers were used for genotyping:

**Table 2.1 List of primers used for genotyping**

| Gene | Forward Primers (5'-3') | Reverse Primers (5'-3') |
|---|---|---|
| Cre | GCG GTC TGG CAG TAA AAA CTA TC | GTG AAA CAG CAT TGC TGT CAC TT |
| Tomato WT | AAG GGA GCT GCA GTG GAG TA | CCG AAA ATC TGT GGG AAG TC |

Mouse mating occurred overnight, and mating was confirmed at E0.5 days by the presence of a vaginal plug. At the time of collection, the pregnant dams were sacrificed by cervical dislocation.

### 2.1.3 Collection of embryos

The tdTomato-expressing embryos were collected at embryonic day (E) 11.5, 13.5, 14.5, 16.5, 18.5 and 20.5. A dissection microscope (Carl Zeiss Stemi SV 11 Apo) facilitated the isolation of the embryos from the uterus. Embryos were subsequently prepared for cryoprocessing and staining (section 2.2), micromass cultures and staining (section 2.3) or single-cell RNA sequencing (scRNA-seq) (section 2.4).

## 2.2 Cryoprocessing

Following collection from the uterus, embryos were fixed for a minimum of 48 hours in 2% paraformaldehyde (PFA). For embryos raised to E16.5 and beyond, decalcification in 14% ethylenediaminetetraacetic acid (EDTA) (Sigma, CAS 60-00-4) in phosphate buffered saline (PBS) was applied after fixation for 4 days to facilitate sectioning. Following fixation +/- decalcification, embryos were saturated in a series of solutions containing D-Sucrose (Fischer Bioreagents, BP-220-10) dissolved in PBS: 10% sucrose/PBS, 20% sucrose/PBS,

30% sucrose/PBS, 40% sucrose/PBS, and 50% sucrose/PBS. Cryoembedding then took place in optimum cutting temperature formulation (OCT) (Sakura Finetek 4583). Using a Leica CM3050 S cryostat, embryos were sectioned at various thicknesses ranging from 10-30μm at approximately -20°C, and were stored at -80°C before staining. It should be noted that frozen sections were used in this study in order to preserve native tdTomato fluorescent reporter protein activity.

### 2.2.1 Staining of cryosections

Sections were thawed for 30 minutes prior to staining, and were then washed three times with PBS. If samples were only stained with DAPI, they would immediately proceed to that step. If the samples were to be stained with agents other than DAPI, samples were placed in $NaBH_4$ (10mg/mL in PBS) for 1 hour, in order to quench autofluorescence. This was followed by three 1-minute rinses in PBS. Samples were blocked overnight in a blocking solution containing 0.25g bovine serum albumin (Sigma Aldrich 7030-100G), 250uL donor goat serum (Gemini Bio-products 100-109) in 20mL PBS. The primary antibody was applied for 1.5 hours (Table 2), the sample was subsequently washed three times for 5-minutes each in PBS, and then the secondary antibody was applied for 1 hour (Table 2.2). This was followed by three 5-minute washes in PBS. DAPI was applied for 5 minutes at a 1:500 dilution in PBS and was washed with three 1-minute rinses in PBS. Coverslips were then applied using Aqua-Poly/Mount mounting media (Polysciences Inc 18606-5). A minimum of n=3 samples and n=3 controls were stained with immunofluorescence for each antibody used.

**Table 2.2 Antibodies**

Antibodies were diluted in blocking solution described in section 2.2.1, at the concentrations indicated below.

| Primary antibody | Manufacturer | Dilution | Corresponding 2° antibody | Manufacturer | Dilution |
|---|---|---|---|---|---|
| **Cluster of differentiation 31 (CD31)** | **BD Pharmingen 550274** | **1:50** | **Alexa Fluor 488** | Invitrogen/Life Technologies A11006 | **1:500** |
| | | | **Alexa Fluor 647** | Invitrogen/Life Technologies A21247 | **1:500** |
| **Neurofilament heavy chain (NFH)** | **Abcam ab4680** | **1:5000** | **Alexa Fluor 647** | Invitrogen/Life Technologies A21449 | **1:500** |
| **SRY-box 9 (SOX9)** | **Santa Cruz Biotechnology sc-20095** | **1:50** | **Alexa Fluor 647** | Invitrogen/Life Technologies A21245 | **1:500** |
| **Type II collagen (COL2A1)** | **Developmental studies hybridoma bank II-II6B3** | **1:50** | **Alexa Fluor 488** | Invitrogen/Life Technologies A11001 | **1:500** |

### 2.2.2 Microscopy for fluorescent imaging

All fluorescent imaging was completed on an Olympus BX63 microscope using an Olympus XM10 camera, and image collection and editing was performed on the Olympus CellSens program. Subsequent editing was completed using Image J software (Version 1.50i, National Institutes of Health).

### 2.2.3. Structure identification

Embryonic anatomy was identified using The Atlas of Mouse Development Revised Edition (Kaufman, 1994).

## 2.3 Micromass cultures

Micromass cultures of cells derived from the mandibular, frontonasal and maxillary prominences at E11.5 were used to study the involvement of *Hic1*$^{+}$ cells in cartilage formation.

### 2.3.1 Dissection for micromass cultures

For micromass cultures, pregnant dams were administered TAM at E10 days and embryos were collected at E11.5 days. Using tissue forceps under aseptic conditions, the maxillary, mandibular and frontonasal processes were dissected from the heads of the 11 embryos under a dissection microscope (Carl Zeiss Stemi SV 11 Apo). These facial processes were isolated by a protocol described by Ralphs. First, vertical cuts were made through the external nostril, to divide the mesial nasal process from the lateral nasal process on the left and right sides of the developing face (Ralphs, 1992). Next, horizontal cuts were applied to the depth of the forebrain, above and below the medial nasal processes (Ralphs, 1992). The section of tissue representing the frontonasal mass was isolated. The maxillary processes were cut away from the adjacent lateral nasal processes and isolated (Ralphs, 1992). For isolation of the mandibular process, cuts were made laterally at the junction between the developing mandible and the side of the head (Ralphs, 1992).

All of the facial processes collected from the 11 embryos were pooled together and collected into one dish of Puck's saline A solution (PSA). The maxillary, mandibular and frontonasal processes were combined together in order to increase cell number, since the cultures need to be plated at such high cellular densities. PSA was prepared by adding 0.4g KCl, 8g NaCl, 0.35g $NaHCO_3$, 1g glucose and enough distilled $H_2O$ to bring total volume to

1L, pH 7.2. PSA was filtered through a sterile Millipore filter into a sterile bottle, and stored at 4$^{o}$C.

### 2.3.2 Tissue processing for micromass cultures

The facial processes were minced with tissue forceps, placed into a 15mL conical tube and centrifuged at 1000 x g for 5 minutes. PSA was aspirated and 2.7mL of PSA containing 10% fetal bovine serum (FBS) (Gibco 12483-020) and 0.3mL Dispase (Roche 04942078001) such that the final concentration of Dispase was 1U/mL. The pieces of facial tissue were incubated for 80 minutes at 37 $^{o}$C with slight shaking, and were gently vortexed every 15 minutes. Three mLs of media (40% Dulbecco's Modified Eagle Medium (DMEM) (Gibco 11965-084) and 60% Ham's F-12 Nutrient Mix (F-12) (Gibco 11765-054)) supplemented with 10% FBS + 1X penicillin-streptomycin (Gibco 15140) and 1X L-glutamine (Gibco 25030081) was added, and the samples were pipetted up and down. Cells were then pelleted at 1000 x g for 5 minutes. Media was removed, 5mL fresh media was added, and cells were re-suspended in media and transferred to a pre-wetted sterile 40 μm nylon mesh cell strainer (Fisherbrand 22363547). Next, the filter was rinsed with 3mL media. Cells were counted using a hemocytometer, centrifuged at 1000 x g for 5 minutes, and re-suspended to a cell density of 2 X $10^{7}$ cells/mL.

### 2.3.3 Micromass cell culture

The cells were mixed in the media and then 10uL was dispensed into the centre of each well of a 24-well plate (Nunc 142475) for Alcian blue staining, or into chamber slides (Nunc Lab-Tek Chamber Slide 177437) for immunostaining with type II collagen (COL2A1). Plated cultures were placed into a well-humidified tissue culture incubator for 1.5 hours, after which point 1mL of media was gently added. Four treatments were administered with n=3

samples per condition: (1) 95% ethanol was used for the control (2) 50nM EC23 (Reinnervate SRP0022) a synthetic retinoid analog was used to inhibit cartilage nodule formation (3) 50nM AGN 194310, a retinoic acid receptor inverse agonist (prepared by University of British Columbia Chemistry Department), was used to promote cartilage nodule formation and (4) 20ng/mL bone morphogenetic protein 4 (BMP4) (Stem Cell Technologies 02524) was applied to promote chondrogenesis. Treatments commenced 24 hours post-seeding, with n=3 samples per condition. Cultures were re-treated at t=3 days, and were fixed at t=4 days. It was expected that cartilaginous nodules would form within 3 days as such nodules were seen by this time point in Ralphs' micromass study (Ralphs, 1992).

### 2.3.4 Staining of micromass cultures with Alcian blue

Samples (n=3) were fixed and stained with Alcian blue which stains cartilage blue, in order to confirm the presence/absence of cartilaginous nodules. To stain the cultures with Alcian blue, media was removed, wells were washed twice with PBS, and then wells were fixed for 10-15 minutes in formalin (1/10 dilution of 37% stock in PBS) (Avantor 2106-01). Wells were washed once with PBS and then once with 0.2M HCl. Next, the Alcian blue stain was applied, using 4 : 1 dilution of 0.2M HCl : 0.5% Alcian blue stock (Acros Organics 400460250) in 95% ethanol. Wells were stained overnight in a well-humidified environment to prevent desiccation. Excess stain was removed by 3-5 washes with 70% ethanol, and then the wells were allowed to dry. 70% ethanol was added to the wells at the time of imaging. Imaging was performed on a Zeiss Axiovert S100 inverted microscope with a QImaging Retiga 1300 camera, and Openlab 5.0.2 software by Improvision. All editing took place on Image J software.

### 2.3.5 Staining of micromass cultures with COL2A1

Cultures were processed for staining with COL2A1 in order to fluorescently identify the cartilaginous nodules, enabling us to view the relationship of *Hic1*$^{+}$ cells to cartilaginous nodules using fluorescent imaging. Samples (n=3) were rinsed once with PBS, and fixed for 10 minutes in 4% PFA in PBS. Next, they were rinsed 4 times for 1 minute each in PBS, and then were permeabilized with 0.1% saponin/PBS (Thermo Fisher Scientific Click-iT Component E) for 20 minutes. Immunofluorescence staining followed the protocol in section 2.2.1, and the microscopy methods in section 2.2.2.

## 2.4 Single-cell RNA sequencing of *Hic1*$^{+}$ and *Hic1*$^{-}$ cells of the head

In order to characterize *Hic1*-expressing cells in craniofacial development, scRNA-seq was performed on cells positive and negative for *Hic1* expression in the head.

### 2.4.1 *Hic1*$^{+}$ and *Hic1*$^{-}$ cell isolation from the head

TAM was administered to 3 pregnant dams at E10, and 19 embryos were collected at E11.5. Heads were dissected from the body of the embryos just below the mandibular prominence, at the level of the second branchial arch. The samples were minced and placed in a solution of 1U/mL Dispase II + 10% FBS in PSA. The digest occurred for 90 minutes in an orbital shaker oven at 70 rpm and 37$^{o}$C, with gentle vortexing every 15 minutes. Cells were filtered in a 40μm cell strainer (Fisherbrand 22363547) and washed in cold fluorescence-activated cell sorting (FACS) buffer (2% FBS/PBS 2mM EDTA). To wash, samples were centrifuged for five minutes at 1000 x g. The supernatant was removed, and cells were re-suspended in FACS buffer, filtered and sorted in a FACS tube (Falcon 352063). FACS then occurred, with sorting for tdTomato. For FACS, an Influx sorter (BD) with SortWare was used to sort the samples at the UBC Flow Cytometry Facility. Purified

tdTomato$^-$ and tdTomato$^+$ samples were visually evaluated for quality control and counted using a hemocytometer. Samples were loaded onto a 10X Chromium Single Cell 3' Controller in house order to generate tagged cDNAs for scRNA-seq analysis. Prepared cDNA libraries were sequenced with an Illumina NextSeq500. Analysis was performed on a 10X Cell Ranger Pipeline and plots generated by K-Means clustering were visualized on Loupe Cell Browser (10X Genomics).

## CHAPTER 3 – RESULTS

### 3.1 Determination of the onset of *Hic1* expression in embryos at E8.5 and E9.5

In order to determine the onset of *Hic1* expression, pregnant dams were administered TAM at E8.5 and subsequently at E9.5 and E10. A minimum of n=3 embryo heads raised to E13.5 days were assessed for each of these TAM administration times. No tdTomato fluorescence was detectable in serial transverse sections anywhere within the head when the TAM was administered at E8.5 and mice were collected at E13.5 (Figure 3.1); however, some autofluorescence attributed to vascular elements was present (Figure 3.1d). When TAM was administered at E9.5, the embryos collected at E13.5 exhibited more tdTomato$^{+}$ cells, which were mainly located at the dorsal aspect of the head, near the neural tube (Figure 3.2). Some tdTomato$^{+}$ cells were already seen in the nasal region at E9.5. Subsequent lineage tracing analysis was performed with TAM injections administered at E10, as this labelled a greater population of cells around the onset of *Hic1* expression.

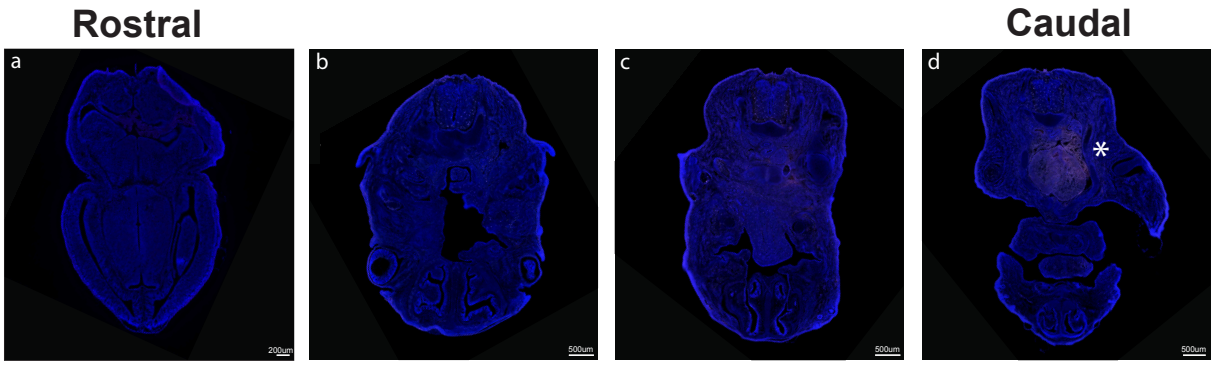


**Figure 3.1 Lineage tracing analysis of embryos with TAM administered at E8.5.** When pregnant dams are administered TAM at E8.5, no tdTomato fluorescent protein is present in the transverse sections of the embryo heads at E13.5 (a-d). * Denotes autofluorescence. Scale bars: **(a)**=200µm **(b-d)** = 500µm.

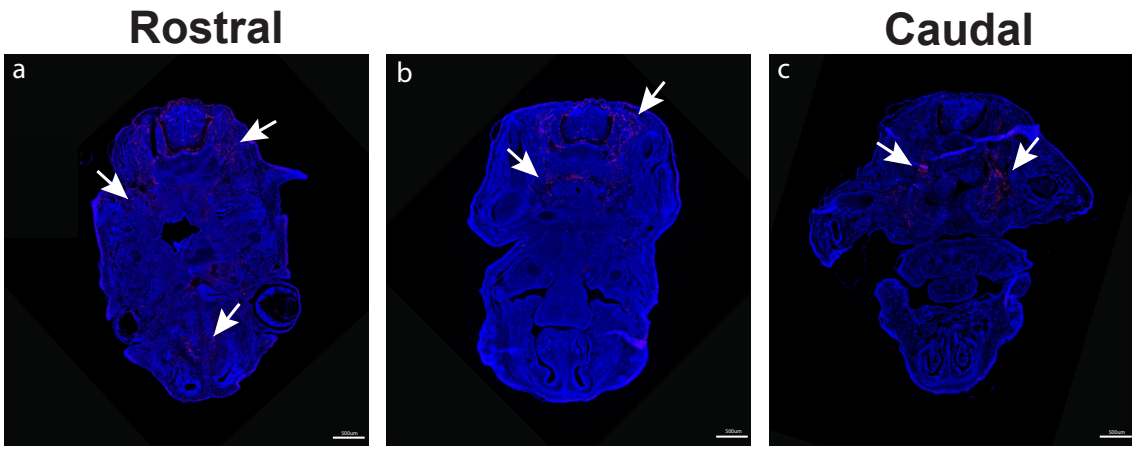


**Figure 3.2 Lineage tracing analysis of embryos with TAM administered at E9.5**.

When pregnant dams are administered TAM at E9.5, tdTomato fluorescent protein begins to become more apparent (arrows), and is more localized in the dorsal aspect of the transverse sections at E13.5 **(a-c).** Some tdTomato can be seen anteriorly in the nasal region **(a).** Scale bars: **(a-c)** = 500µm.

## 3.2 Lineage tracing analysis of *Hic1*-expressing cells

Lineage tracing analysis was performed on developing embryo heads to demonstrate the presence of tdTomato$^+$ *Hic1*-expressing cells and their progeny in transverse, coronal and sagittal sections at various time-points in development. For each time-point, a minimum of n=3 embryo heads were assessed, with TAM administration at E10. Figures 3.3, 3.4, 3.5, 3.6, and 3.7 demonstrate the migration of *Hic1*$^+$ cells labelled at E10 in addition to their progeny at E11.5, E13.5, E14.5, E16.5 and E18.5, respectively. Figure 3.8 includes coronal sections from E13.5-E18.5, and Figure 3.9 includes sagittal sections from E11.5-E18.5. Figure 3.10 demonstrates transverse sections at E20.5.

From lineage tracing analysis, we can see that *Hic1*$^+$ cells and/or their progeny contribute to various mesenchymal tissues. Skeletally, tdTomato$^+$ cells contribute to the mesenchyme within the facial/masticatory muscles, tendon, tongue, meninges, nasal cartilage and connective tissue, the periphery of the hyoid bone and the cartilage primordium of the vertebrae. These tdTomato$^+$ cells, however, were selective in the cartilages they contribute to, as they were absent from Meckel's cartilage, the mandibular condyle, the majority of the hyoid, the incus and stapes of the middle ear, and the anterior and posterior cranial base. tdTomato$^+$ cells were also absent from the developing palatal shelves, and were not present in the maxilla nor in the mandible. With respect to the nervous system, tdTomato$^+$ cells were evident throughout the brain, including within the pituitary gland and hypothalamus. These cells were also located within various ganglia, and were also seen around nerves, including the right and left optic nerves. With respect to the eyes, tdTomato$^+$ cells were present in the hyaloid cavity, which is highly vascular, and in the cornea. In terms of glandular tissues, tdTomato$^+$ cells were seen in the stroma surrounding salivary glands, and mucous glands.

Dentally, *Hic1*$^{+}$ cells were present surrounding the developing teeth in the periodontal ligament region, and within the developing dental papilla/pulp.

**A.**

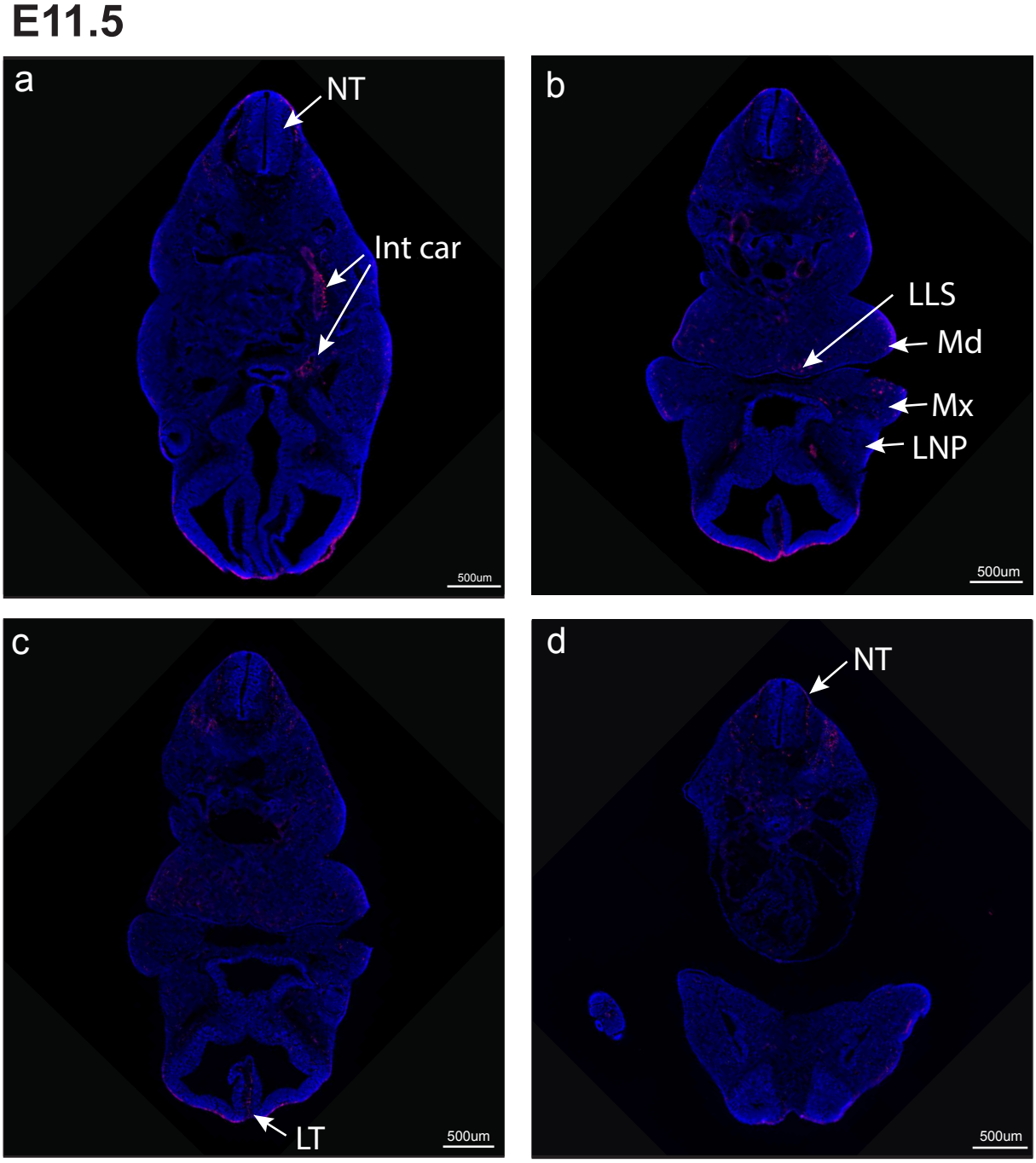

**B.**

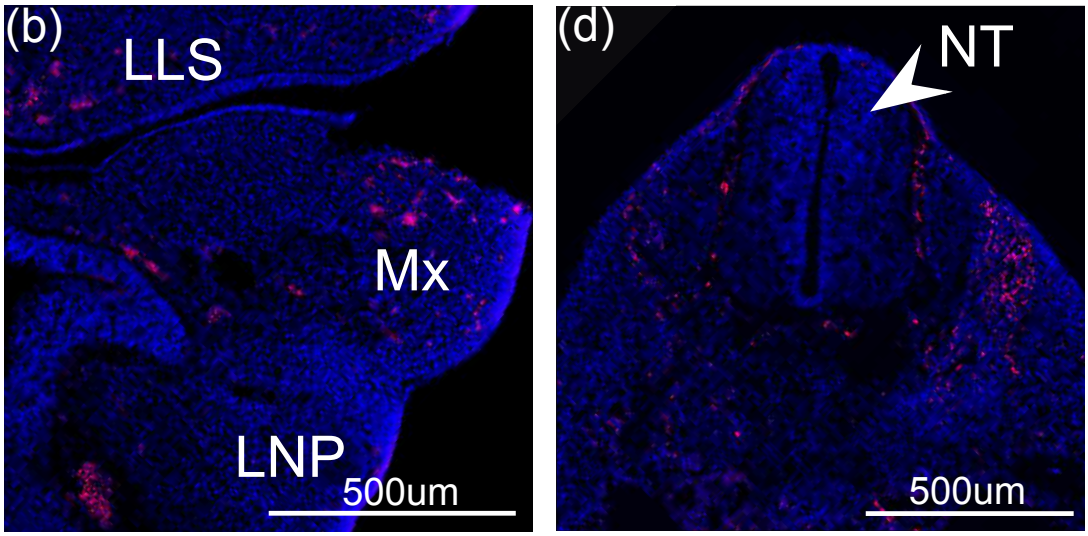


**Figure 3.3 Lineage tracing analysis of transverse sections of embryos at E11.5.**

**A.** Sections progress from rostral **(a)** to caudal **(d). (a)** tdTomato$^{+}$ cells are present outside of the neural tube (NT) (arrow) and internal carotid artery (Int car) (arrow). **(b)** tdTomato$^{+}$ cells are present within the lateral lingual swelling (LLS) (arrow) which later forms the anterior 2/3 of the tongue. In this section, the maxillary (Mx) and mandibular (Md) components of the first branchial arch (arrows), as well as the lateral nasal processes (LNP) (arrow) can be seen. **(c)** tdTomato$^{+}$ signal is seen at the lamina terminalis (LT) (arrow) which is highly vascular. **(d)** tdTomato$^{+}$ cells present around the neural tube (NT) (arrow). **B.** High magnification images extracted from the sections in part A. All scale bars = 500μm.

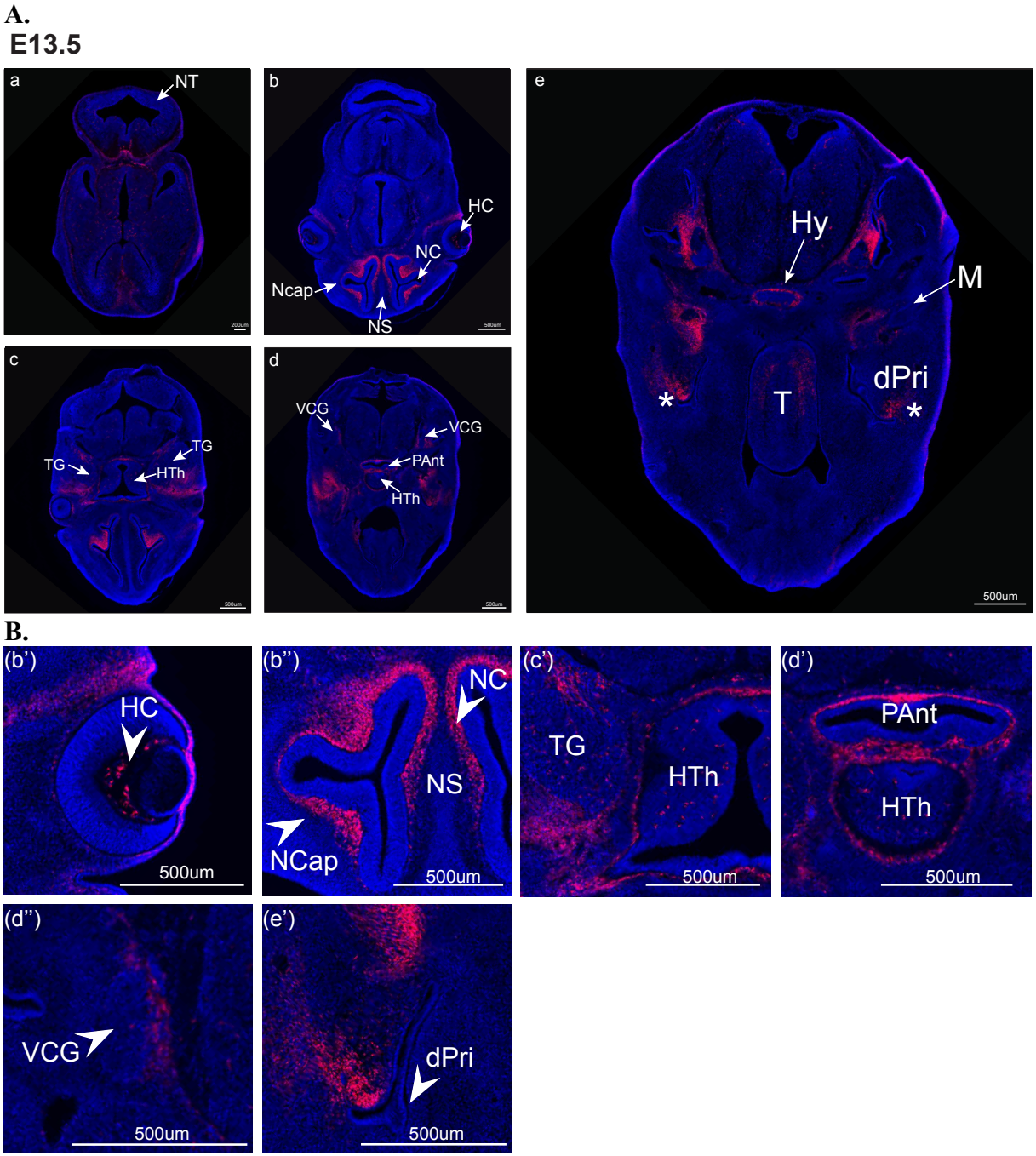


**Figure 3.4 Lineage tracing analysis of transverse sections of embryos at E13.5.**

**A.** Sections progress from rostral **(a)** to caudal **(e)**. **(a)** Rostrally, tdTomato$^{+}$ cells are seen throughout the brain tissue. NT=neural tube (arrow). **(b)** tdTomato$^{+}$ cells are present within the nasal connective tissue (NC) (arrow) and are relatively absent from the nasal septum (NS) (arrow) and nasal capsule (Ncap) (arrow). tdTomato$^{+}$ are located within the hyaloid cavity

(HC) of the eye, which is highly vascular (arrow). **(c)** tdTomato$^{+}$ cells exist in the trigeminal ganglia (TG) (arrows) and hypothalamus (HTh) (arrow). **(d)** tdTomato$^{+}$ cells are evident in the hypothalamus (HTh) (arrow), the pars anterior of the pituitary gland (PAnt) (arrow), in addition to the vestibulocochlear ganglia (VCG) (arrows). **(e)** tdTomato$^{+}$ cells are present in the tongue (T) (arrow), in the mesenchyme surrounding the dental primordium (dPri) (indicated with *) and surrounding the body of the hyoid (Hy) (arrow). These cells are absent from Meckel's cartilage (M) (arrow). **B.** High magnification images extracted from the sections in part A. Scale bars: **(a)** = 200μm, **(b-e)** = 500μm.

A.

# E14.5

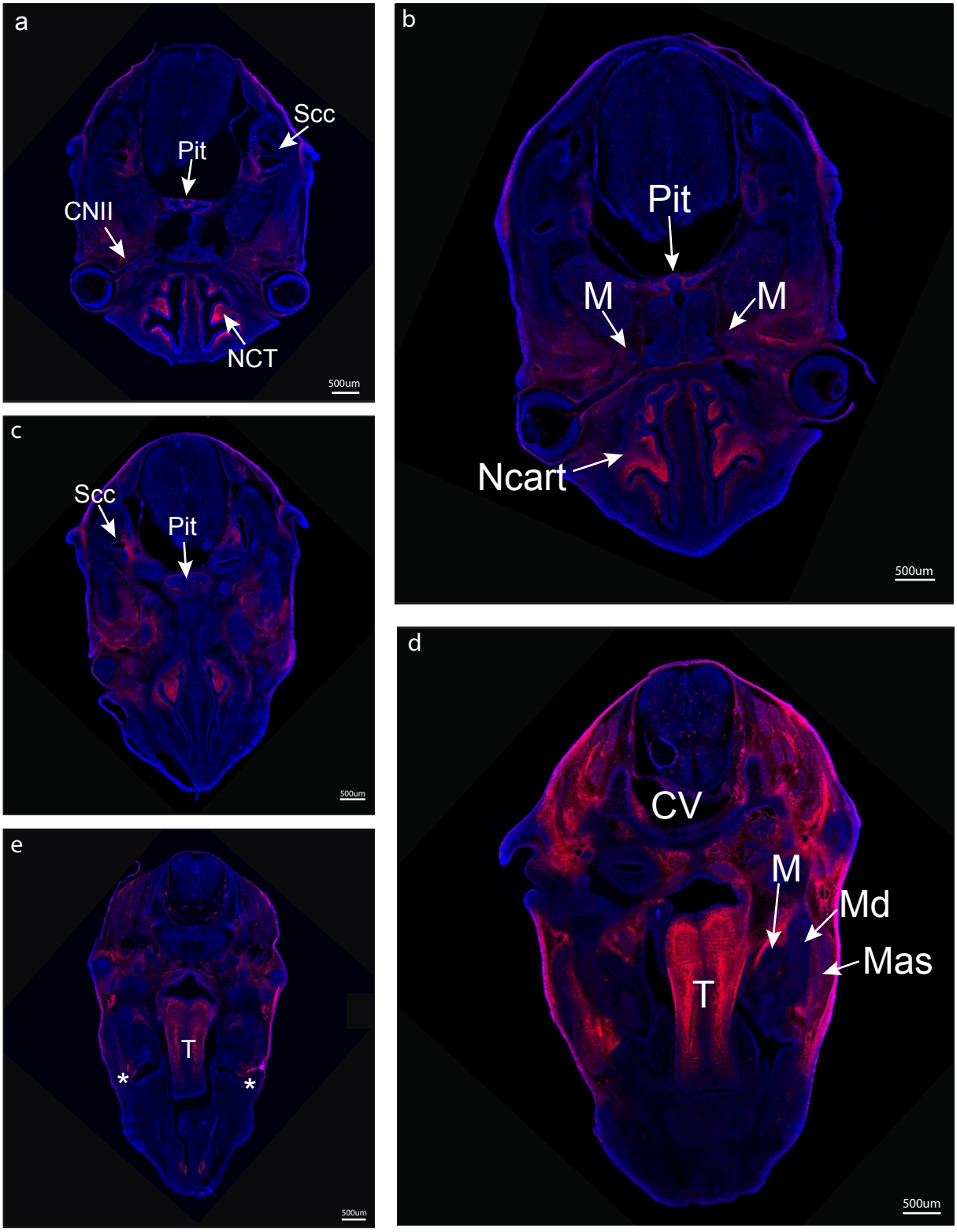
a
Scc
Pit
CNII
NCT
500um
b
Pit
M
M
Ncart
500um
c
Scc
Pit
500um
d
CV
M
Md
Mas
T
500um
e
T
*
*
500um

**B.**

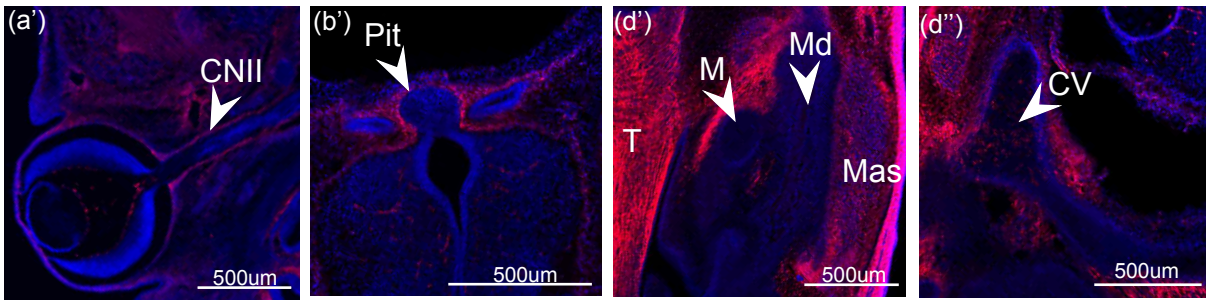


**Figure 3.5 Lineage tracing analysis of transverse sections of embryos at E14.5.**

**A.** Sections progress from rostral **(a)** to caudal **(e)**. **(a-c)** tdTomato$^{+}$ cells are present within and around the pituitary gland (Pit) (arrow), nasal connective tissue (NCT) (arrow) and nasal cartilage (Ncart) (arrow), the optic nerve (CNII) (arrow) and medial to the semicircular canals of the inner ear (SCC) (arrow). They are absent from Meckel's cartilage (M) (arrow). **(d-e)** tdTomato$^{+}$ cells are present in the developing tongue (T), more so posteriorly than anteriorly, in the masseter muscles (Mas) (arrow), and in the cervical vertebrae (CV) (arrow in d"). tdTomato$^{+}$ cells are absent from the mandible (Md) (arrow), which is ossifying in areas. A group of tdTomato$^{+}$ cells is seen lateral to the developing lower molars (as denoted by *). **B.** High magnification images extracted from the sections in part A. Scale bars: **(a-e)** = 500μm.

A.

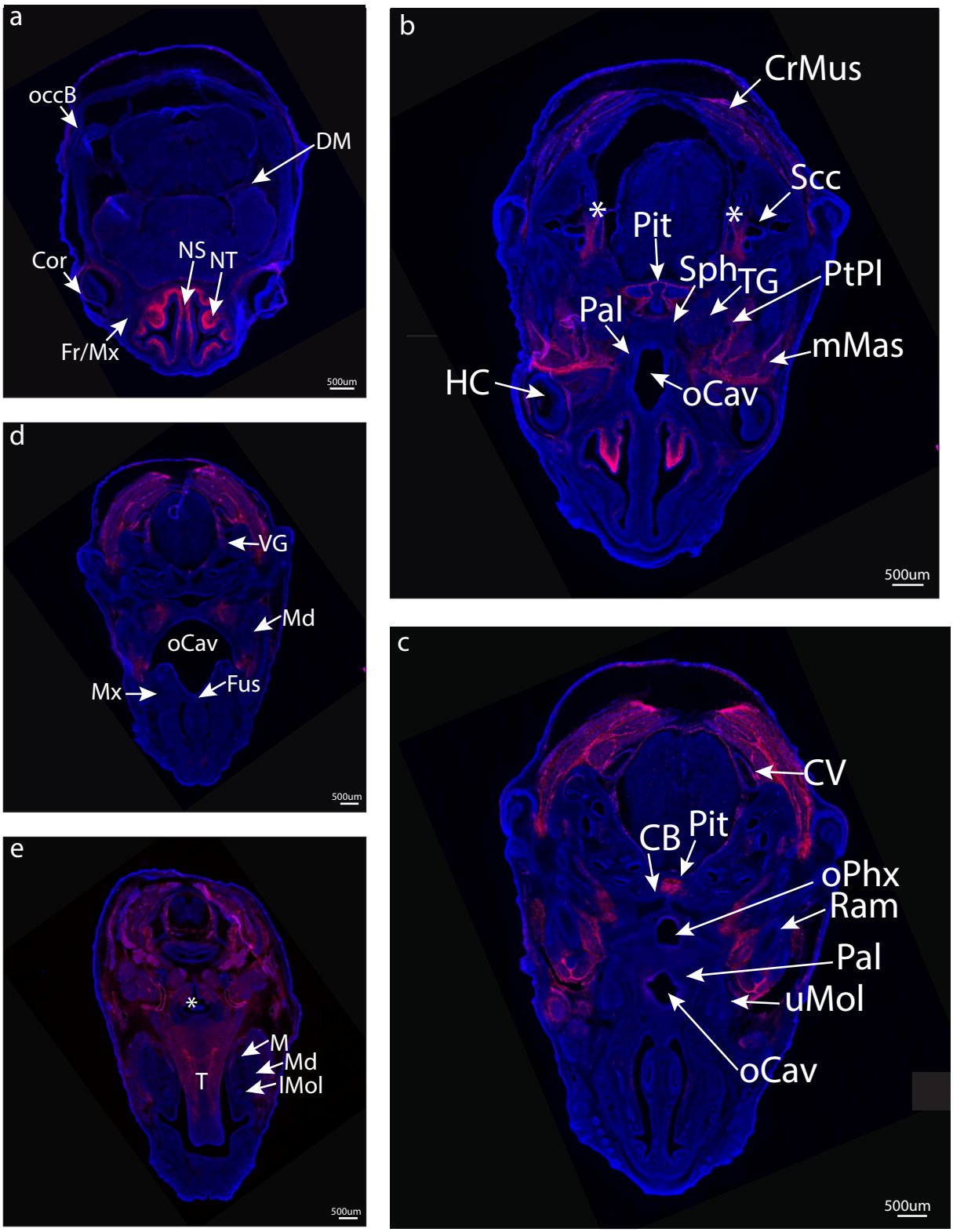
E16.5
a
occB
DM
Cor
NS
NT
Fr/Mx
500um
b
CrMus
Scc
*
Pit
*
Sph
TG
PtPl
Pal
mMas
HC
oCav
500um
d
VG
Md
oCav
Mx
Fus
500um
c
CV
CB
Pit
oPhx
Ram
Pal
uMol
oCav
500um
e
*
M
Md
T
lMol
500um

**B.**

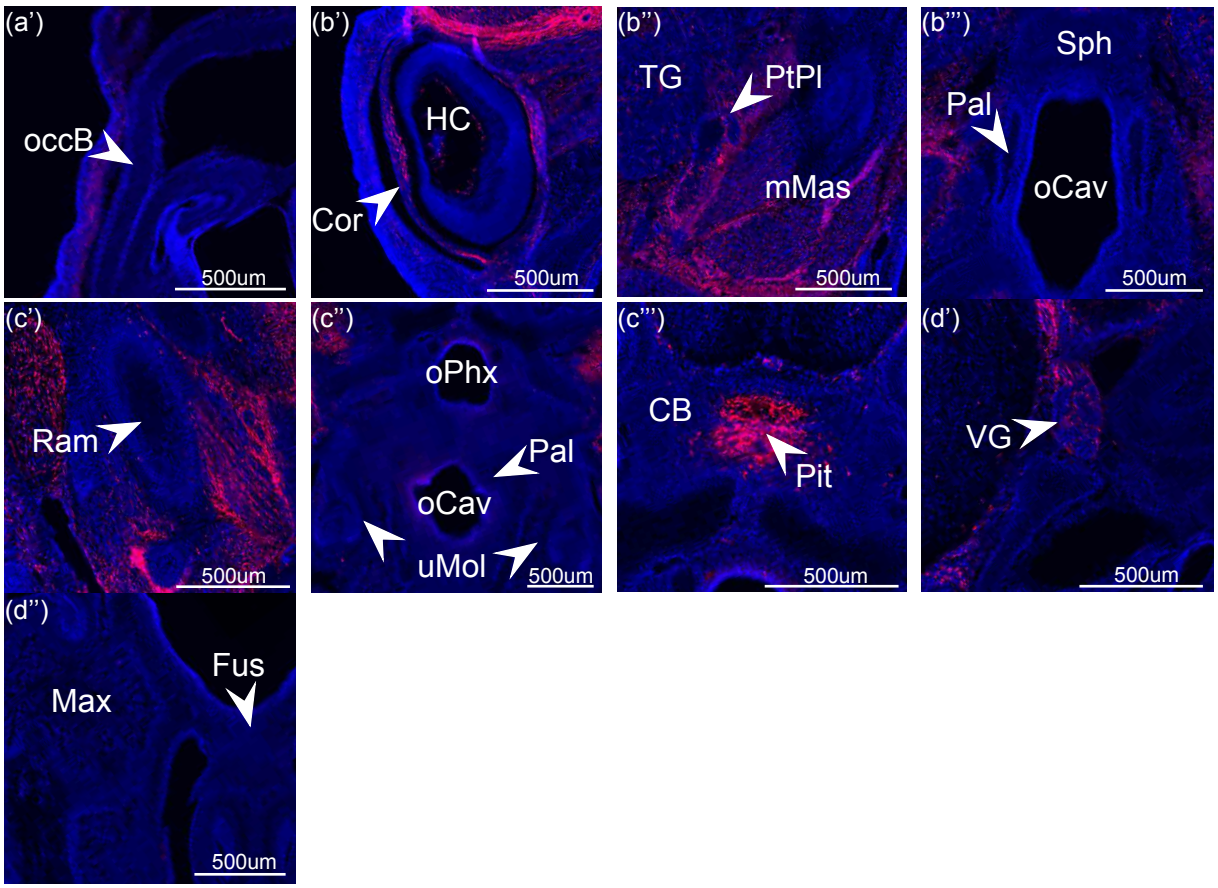


**Figure 3.6 Lineage tracing analysis of transverse sections of embryos at E16.5.**

**A.** Sections progress from rostral (a) to caudal (e). **(a)** tdTomato$^{+}$ cells are absent from the cartilaginous primordium of the occipital bone (occB) (arrow) and from the orbital part of the frontal/Mx bone (Fr/Mx) (arrow). tdTomato$^{+}$ cells are present in the nasal connective tissue, including areas of the nasal septal cartilage (NS) (arrow) and nasal turbinates (NT) (arrow). tdTomato$^{+}$ signal is absent from the nasal epithelium, and is localized to the underlying connective tissue. In the eye, the tdTomato$^{+}$ cells are visible in the cornea (Cor) (arrow), and what appear to be the extrinsic ocular muscles adjacent to the eye. tdTomato$^{+}$ cells exist within the dura mater (DM) (arrow). **(b)** tdTomato$^{+}$ is seen in the cranial muscles overlying the skull (CrMus) (arrow), the masticatory muscles (mMas) (arrow), and bilaterally in a cartilaginous structure located mesial to these muscles, the lateral pterygoid plate (PtPl)

(arrow). tdTomato$^+$ cells are present in and around the developing pituitary gland (Pit) (arrow), and are absent from, but surround the sphenoid (Sph) (arrow), anterior to the pituitary, that forms the anterior cranial base. The tdTomato$^+$ cells are absent from the palatal shelves of the maxilla (Pal) (arrow), located on either side of the oral cavity (oCav) (arrow). In the eye, the tdTomato$^+$ cells can be seen in the hyaloid cavity (HC) (arrow). There is a population of tdTomato$^+$ cells in the cartilage located medial to the semicircular canals (Scc) (arrow), and in the vestibulocochlear ganglion (*). tdTomato cells are present in the trigeminal ganglion (TG) (arrow)**. (c)** tdTomato$^+$ cells are located in the cartilage of the cervical vertebrae (CV) (arrow). These cells are absent from the upper molars (uMol) (arrow) and surrounding mesenchyme, the ramus (Ram) (arrow), palate (Pal) (arrow), and cranial base (CB) (arrow) surrounding the pituitary (Pit) (arrow). oCav=oral cavity (arrow), oPhx=oropharynx (arrow). **(d)** Ossification within the maxilla (Mx) is evident at this stage (arrow). There is no tdTomato$^+$ signal present here, nor is it present at the site of fusion (Fus) between the nasal septum and primary palate (arrow). Ossification is also evident within the mandible (Md) (arrow), in which no tdTomato$^+$ cells are present at this time. tdTomato$^+$ cells are present in the vagal ganglion (VG) (arrow). oCav=oral cavity. **(e) *** denotes the common entrance from the pharynx into the esophagus and trachea. tdTomato$^+$ cells are present in the muscle posterior to this space. tdTomato$^+$ cells are highly present within the tongue (T), and are more prevalent in the posterior tongue than the anterior tongue. There are no tdTomato$^+$ cells seen in the developing lower molars (lMol) (arrow), ossifying mandible (Md) (arrow), or Meckel's cartilage (M) (arrow) at this time. **B.** High magnification images extracted from the sections in part A. Scale bars: **(a-e)** = 500μm.

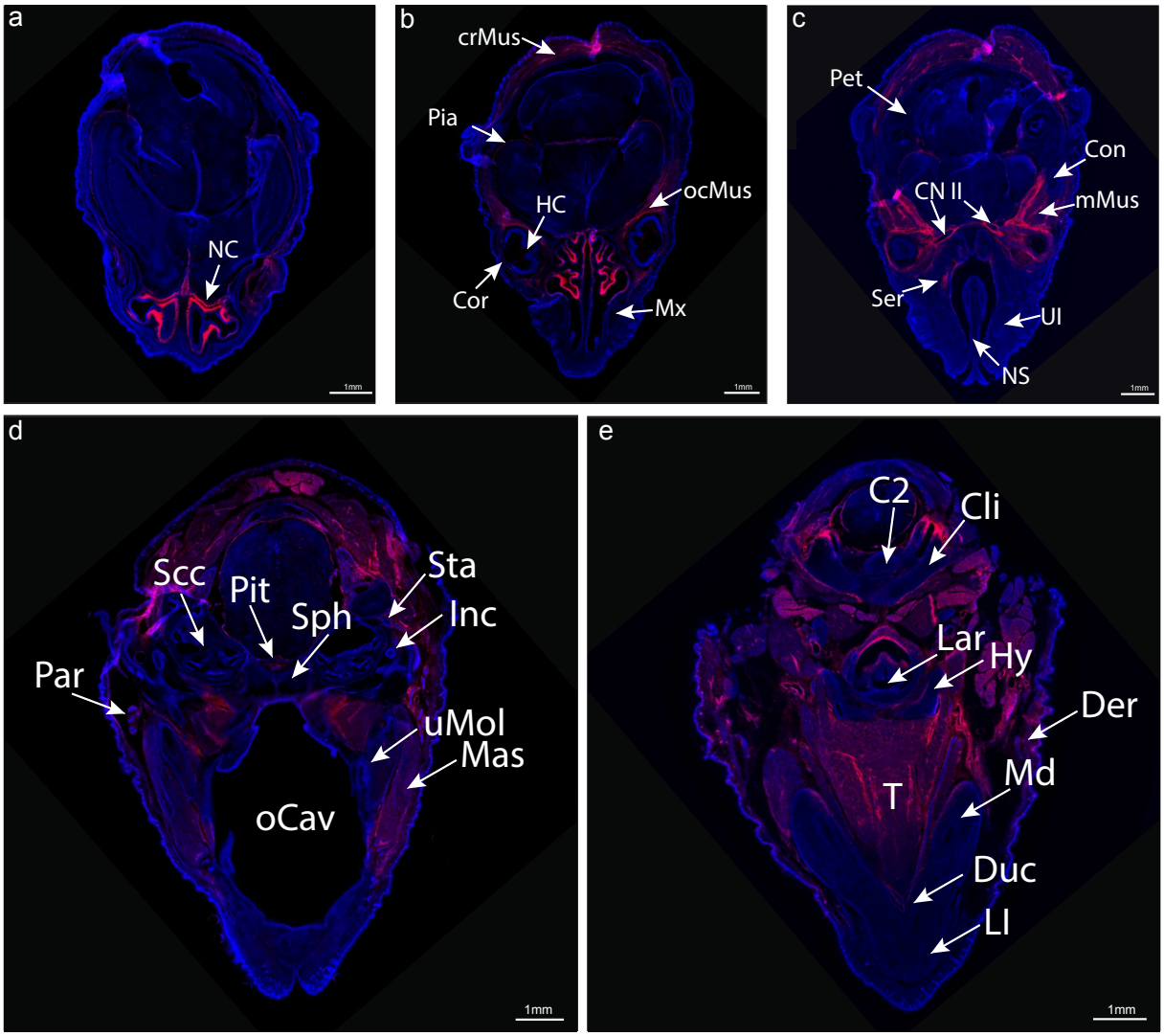


**Figure 3.7 Lineage tracing analysis of transverse sections of embryos at E18.5.**

**A.** Sections progress from rostral **(a)** to caudal **(e)**. **(a)** tdTomato$^{+}$ cells are generalized throughout the brain, and localized within the nasal cartilage (NC) (arrow) and the surrounding nasal connective tissue. They are absent from the nasal epithelium. **(b)** tdTomato$^{+}$ cells are present within the connective tissue surrounding the nasal mucous glands, within the ocular muscles (ocMus) (arrow), the hyaloid cavity (HC) (arrow) and cornea (Cor) (arrow) of the eye. Finally, tdTomato$^{+}$ cells are present within the muscles surrounding the

cranium (crMus) (arrow) and the pia mater overlying the brain (Pia) (arrow). tdTomato$^+$ cells are absent from the maxilla (Mx) (arrow). **(c)** tdTomato$^+$ cells are seen surrounding the serous glands (Ser) (arrow) associated with the lateral wall of the middle meatus, within the muscles of mastication (mMus) (arrow) and surrounding the optic nerve (CN II) (arrows). tdTomato$^+$ is not present in the petrous part of the temporal bone (Pet) (arrow), nor in the condyle (Con) (arrow). Few tdTomato$^+$ cells are seen surrounding the upper incisor (UI) (arrow) but are absent from the contralateral UI. These cells are not present in the nasal septum (NS) (arrow) at this transverse level. **(d)** tdTomato$^+$ cells are present in the developing pituitary (Pit) (arrow). Skeletally, tdTomato$^+$ signal is absent from the cartilage primordium of the basisphenoid (Sph) (arrow), stapes (Sta) (arrow), and incus (Inc) (arrow). tdTomato$^+$ signal is highly present in the muscles of mastication, including the masseter (Mas) (arrow) and the pterygoids. tdTomato$^+$ signal is present in the salivary gland stroma of the parotid gland (Par) (arrow). There are very few tdTomato$^+$ cells around the semicircular canals of the inner ear (Scc) (arrow), and only a few around the upper molar (uMol) (arrow). oCav= oral cavity. **(e)** tdTomato$^+$ cells are abundant within the tongue (T), and are seen around the ductal openings of the sublingual and submandibular glands (Duc) (arrow). tdTomato$^+$ is absent from the mandible (Md) (arrow), the laryngeal cartilage (Lar) (arrow) and from the cartilage primordium of the hyoid (Hy) (arrow). Few tdTomato$^+$ cells are seen surrounding the clivus of the basioccipital bone (Cli) (arrow), particularly around the lateral aspects, and none are visible within the odontoid process of the second cervical vertebra (C2) (arrow). tdTomato$^+$ is generally located within muscles, including the laryngeal muscles, and is also located in the dermis (Der) (arrow). Finally, no tdTomato$^+$ is seen near the lower incisors (LI) (arrow). Scale bars: **(a-e)** = 1mm.

**A.**

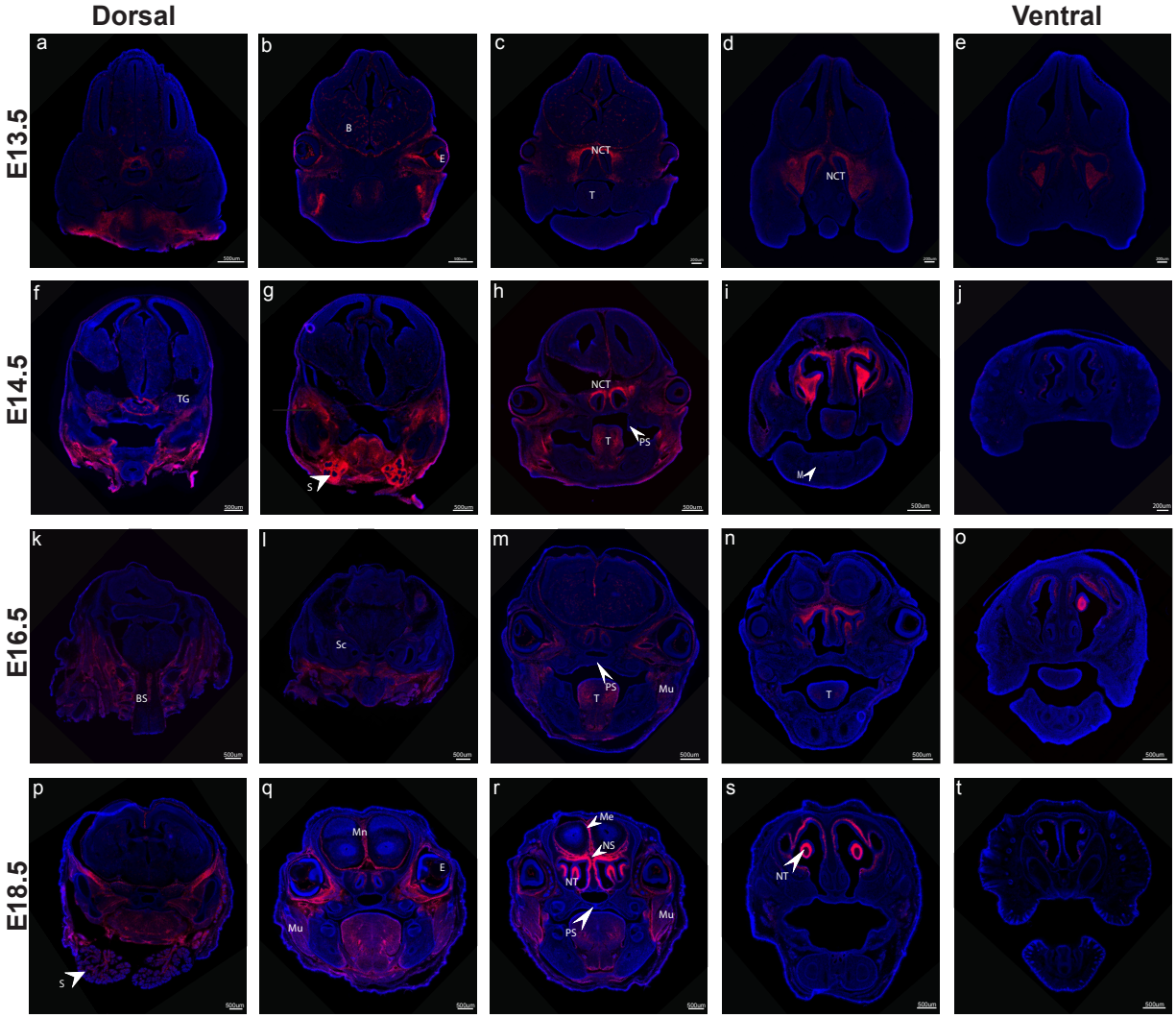
Dorsal
Ventral
E13.5
E14.5
E16.5
E18.5
a
b
B
E
c
NCT
T
d
NCT
e
f
TG
g
S
h
NCT
T
PS
i
M
j
k
BS
l
Sc
m
PS
T
Mu
n
T
o
p
S
q
Mn
E
Mu
r
Me
NS
NT
PS
Mu
s
NT
t

**B.**

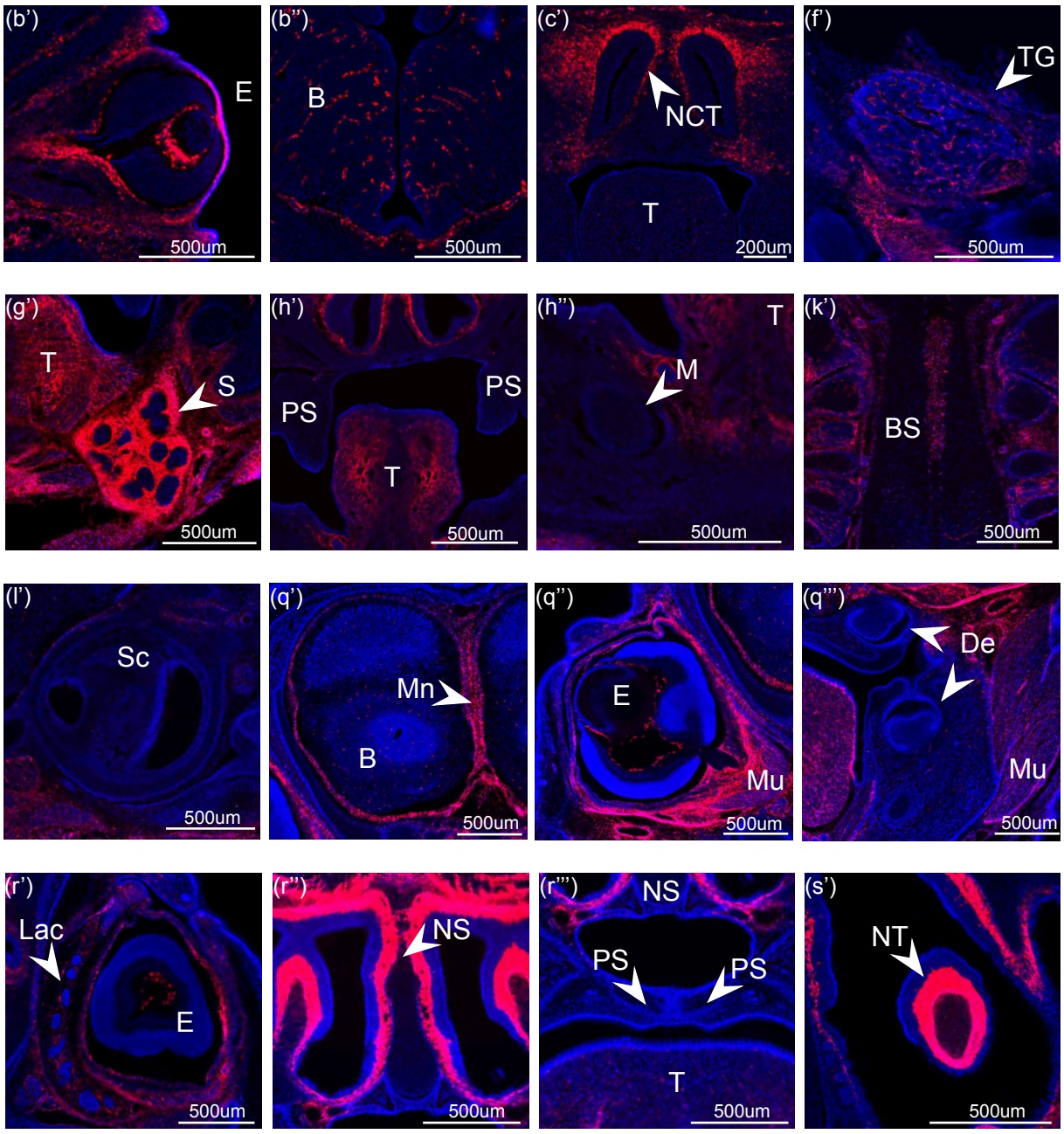


**Figure 3.8 Lineage tracing analysis of coronal sections of embryos at E13.5, E14.5, E16.5, and E18.5. A.** tdTomato$^{+}$ cells are present within the nasal turbinates (NT) (arrow), nasal septum (NS) (arrow), nasal connective tissues (NCT), eyes (E), tongue (T), muscular compartments (Mu), meninges (Mn) (arrow), salivary parenchyma (S) (arrow), brain (B), brain stem (BS) and trigeminal ganglia (TG) (arrow). tdTomato$^{+}$ cells are absent from the

developing palatal shelves (PS) (arrows), Meckel's cartilage (M) (arrow), and the semicircular canals of the middle ear (Sc) from E13.5-E18.5. De: teeth (arrows), Lac: lacrimal gland (arrow). **B.** High magnification images extracted from the sections in part A. Scale bars: **(a-b, f-i, k-t)** = 500μm, **(c-e, j)** = 200μm.

A.

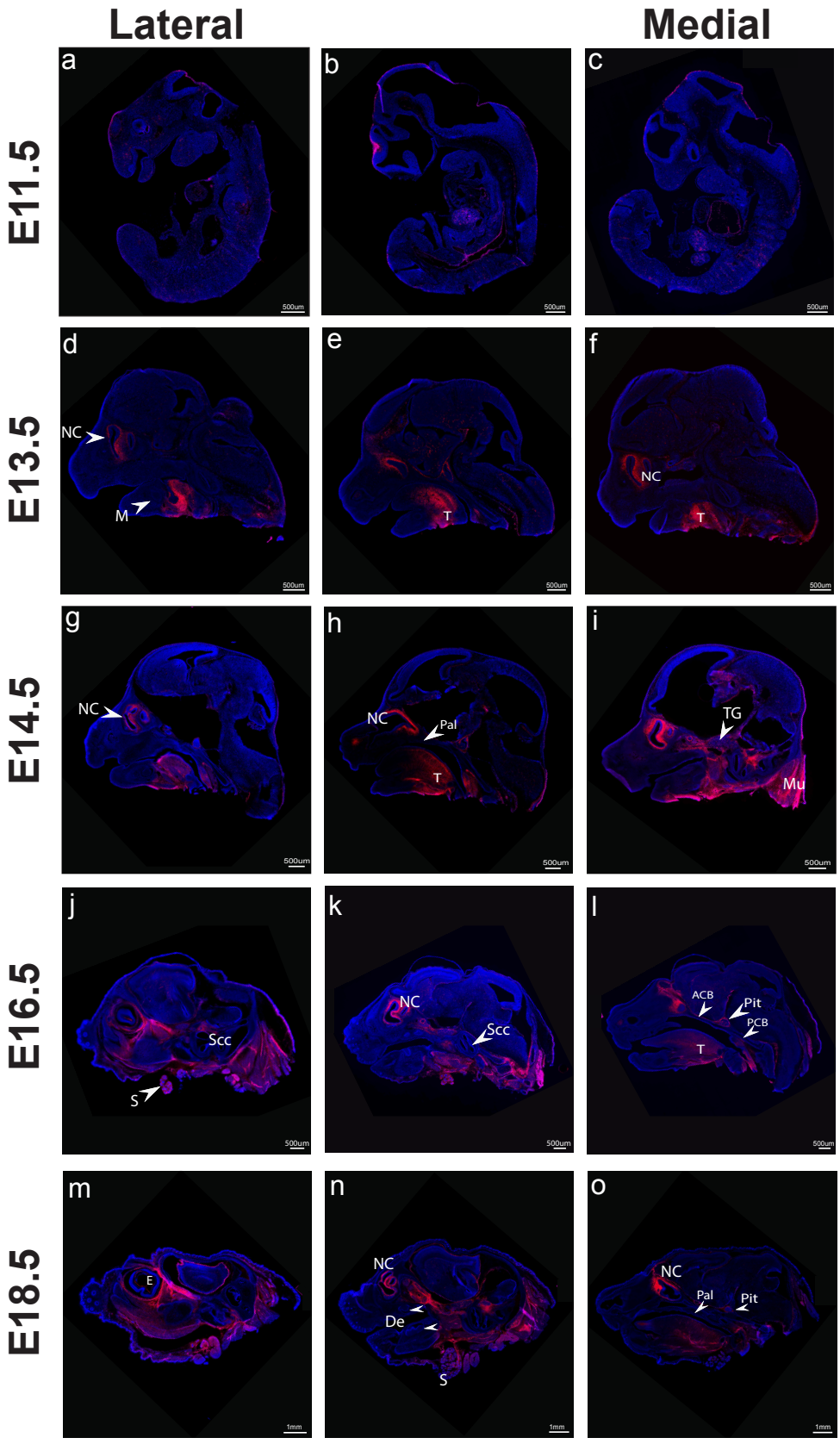
Lateral
Medial
E11.5
E13.5
E14.5
E16.5
E18.5
a
b
c
d
e
f
g
h
i
j
k
l
m
n
o
NC
M
T
Pal
TG
Mu
Scc
S
ACB
Pit
PCB
E
De
500um
1mm

**B.**

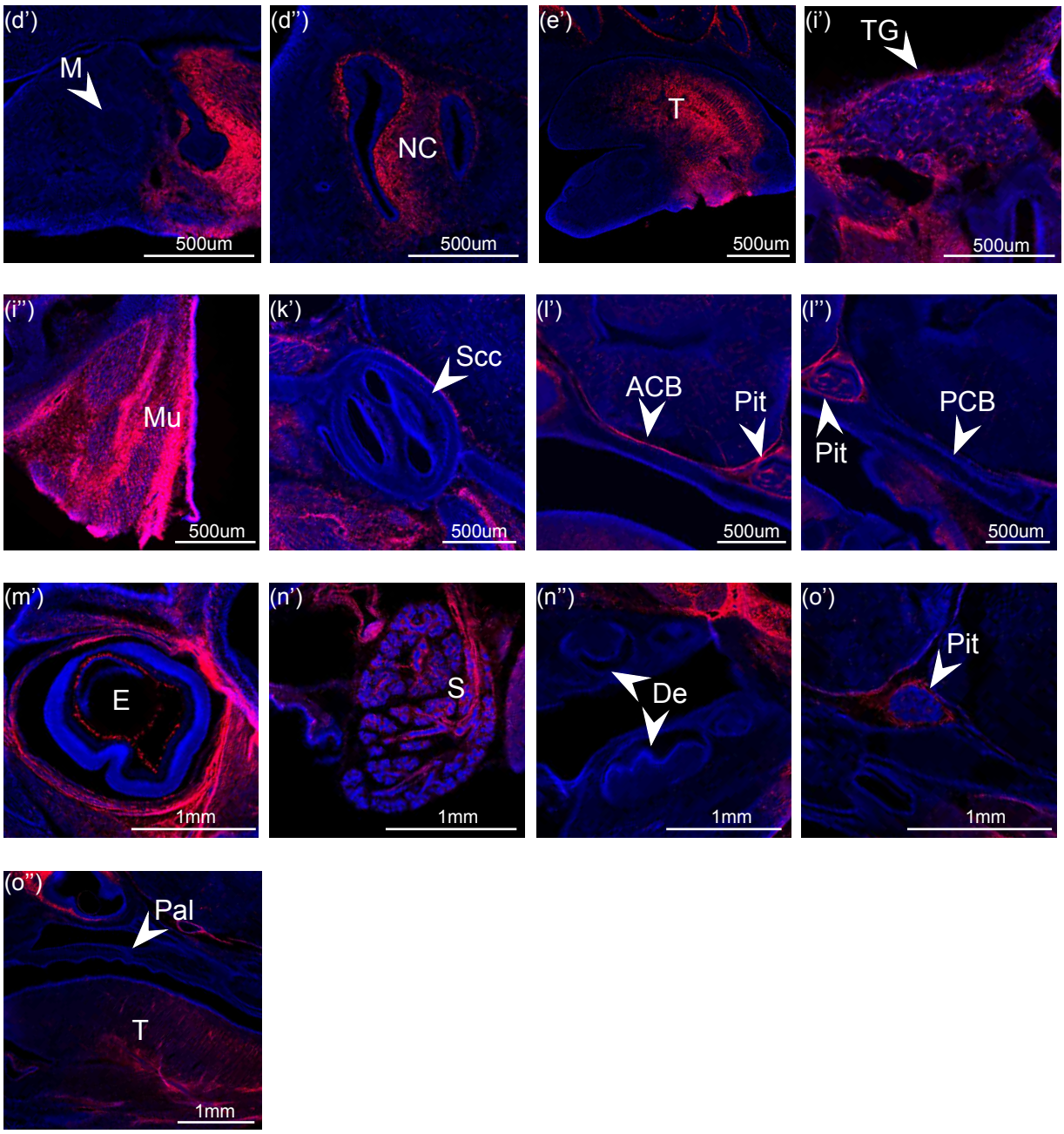


**Figure 3.9 Lineage tracing analysis of sagittal sections of embryos at E11.5, E13.5, E14.5, E16.5 and E18.5. A.** At E11.5 **(a-c)**, there are no distinct concentrations of tdTomato$^{+}$ cells. By E13.5 **(d-f),** tdTomato$^{+}$ cells are concentrated in the nasal cavity (NC) (arrow) and tongue (T) regions. There is a greater concentration of tdTomato$^{+}$ cells in the posterior tongue, as compared to in the anterior tongue **(h, l).** The trigeminal ganglion (TG) (arrow),

muscular compartments (Mu) and salivary gland stroma (S) (arrow) also have tdTomato$^{+}$ cells present. There is a concentration of tdTomato$^{+}$ cells around the developing pituitary gland (Pit) (arrow) **(h, l).** Note the absence of tdTomato$^{+}$ cells from the developing palate (Pal) (arrow) **(h, l, o),** Meckel's cartilage (M) (arrow) **(d),** semicircular canals of the inner ear (Scc) (arrow) **(j, k),** the developing dentition (De) (arrows) **(n),** and the developing anterior and posterior cranial base (ACB, PCB) (arrows) **(l).** E: eye **(m). B.** High magnification images extracted from the sections in part A. Scale bars: **(a-l)** = 500μm, **(m-o)** = 1mm.

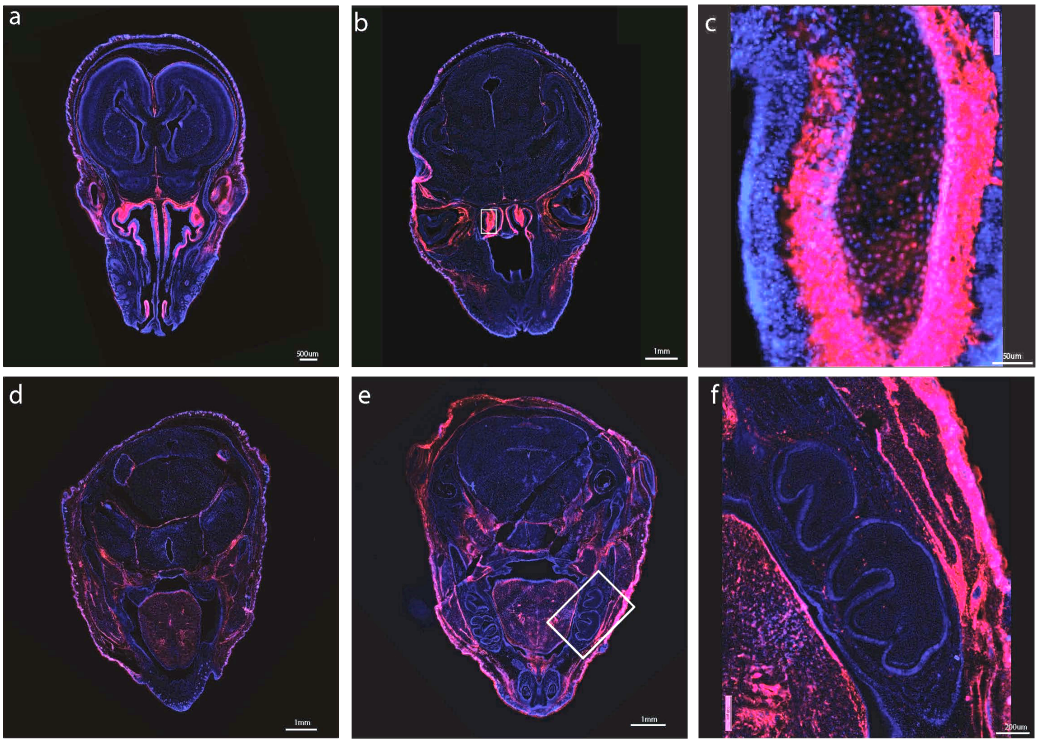


**Figure 3.10 Lineage tracing analysis of E20.5 embryos in transverse sections.**

TAM was administered to the pregnant dam at E11. tdTomato$^{+}$ cells are seen in the nasal structures including the nasal cartilage **(a-c)** (box in **b**, magnified in **c**), the tongue, muscular compartments, meninges **(d)** and within and adjacent to the developing teeth (box in **e,** rotated and magnified in **f**). **(f)** The tdTomato$^{+}$ cells are present in the developing dental papilla/pulp within the teeth, and in the surrounding region, which may become the periodontal ligament. Scale bars: **(a)** = 500µm, **(b, d, e)** = 1mm, **(c)** = 50µm, **(f)** = 200µm.

### 3.3 Immunofluorescence staining of embryos for CD31, SOX9, and NFH

The relationship of tdTomato$^+$ cells to cartilage and vessels was explored in transverse sections by staining sections for cluster of differentiation 31 (CD31) and SOX9, respectively (Figure 3.11, 3.12). tdTomato$^+$ cells were found to be positive for both SOX9 and CD31. The co-localization of tdTomato$^+$ and CD31$^+$ cells is especially evident in the vessels in and around the eye (Figure 3.12). With respect to cartilage, tdTomato$^+$ cells were present within the vertebral cartilage at E13.5 (Figure 3.11). The tdTomato$^+$ cells were not highly concentrated in and around the nasal regions at this time point, but it should be noted that TAM was administered at E9.5 for the samples included in Figure 3.11.

Neurofilament (NFH) staining demonstrated that tdTomato$^+$ cells were located around neurons within the brain, cervical spinal nerves, brainstem, and spinal cord (Figure 3.13).

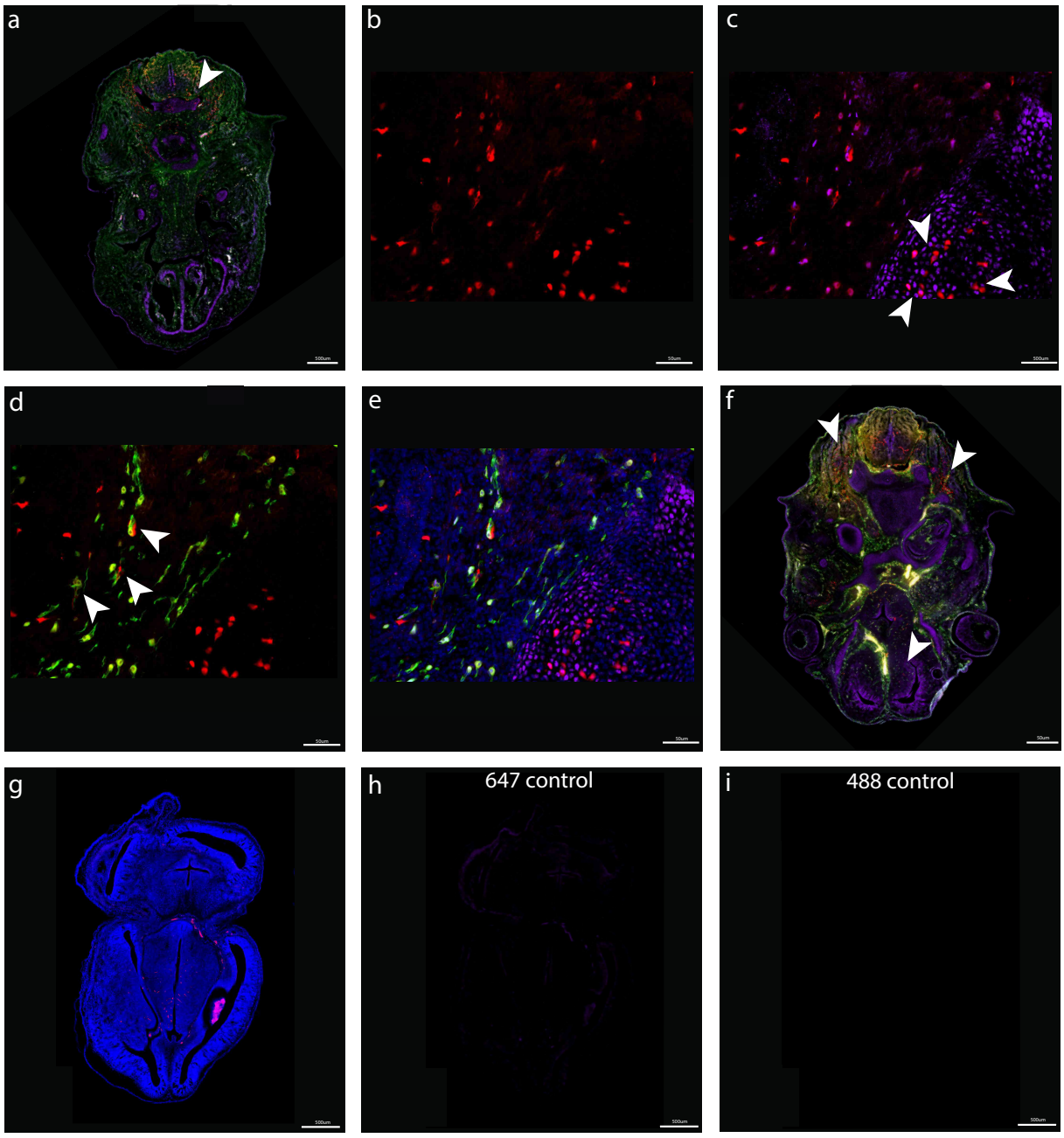


**Figure 3.11 SOX9 and CD31 staining of E13.5 embryos with TAM administered at E9.5**. All sections are transverse. **(a)** Overlay of SOX9, CD31 and tdTomato. tdTomato$^{+}$ cells are localized in the dorsal aspect of the developing head (arrow). **(b)** tdTomato$^{+}$ cells from the vertebral cartilage and surrounding area indicated by the arrow in **(a)**. **(c)** Co-localization of tdTomato and SOX9 in cells in the vertebral cartilage (arrows). **(d)** Co-localization of tdTomato and CD31 cells in cells adjacent to the vertebral cartilage (arrows). **(e)** Overlay of

SOX9, CD31, tdTomato and DAPI. **(f)** Another transverse section demonstrated the posterior localization of the tdTomato$^{+}$ cells at E13.5 (arrows). **(g)** Overlay control with DAPI, Alexa Fluor 647 and Alexa Fluor 488, with no primary antibodies. **(h)** Alexa Fluor 647 control alone with no primary antibody. **(i)** Alexa Fluor 488 control alone with no primary antibody. Scale bars: **(a, f-i)** = 500μm, **(b-e)** = 50μm.

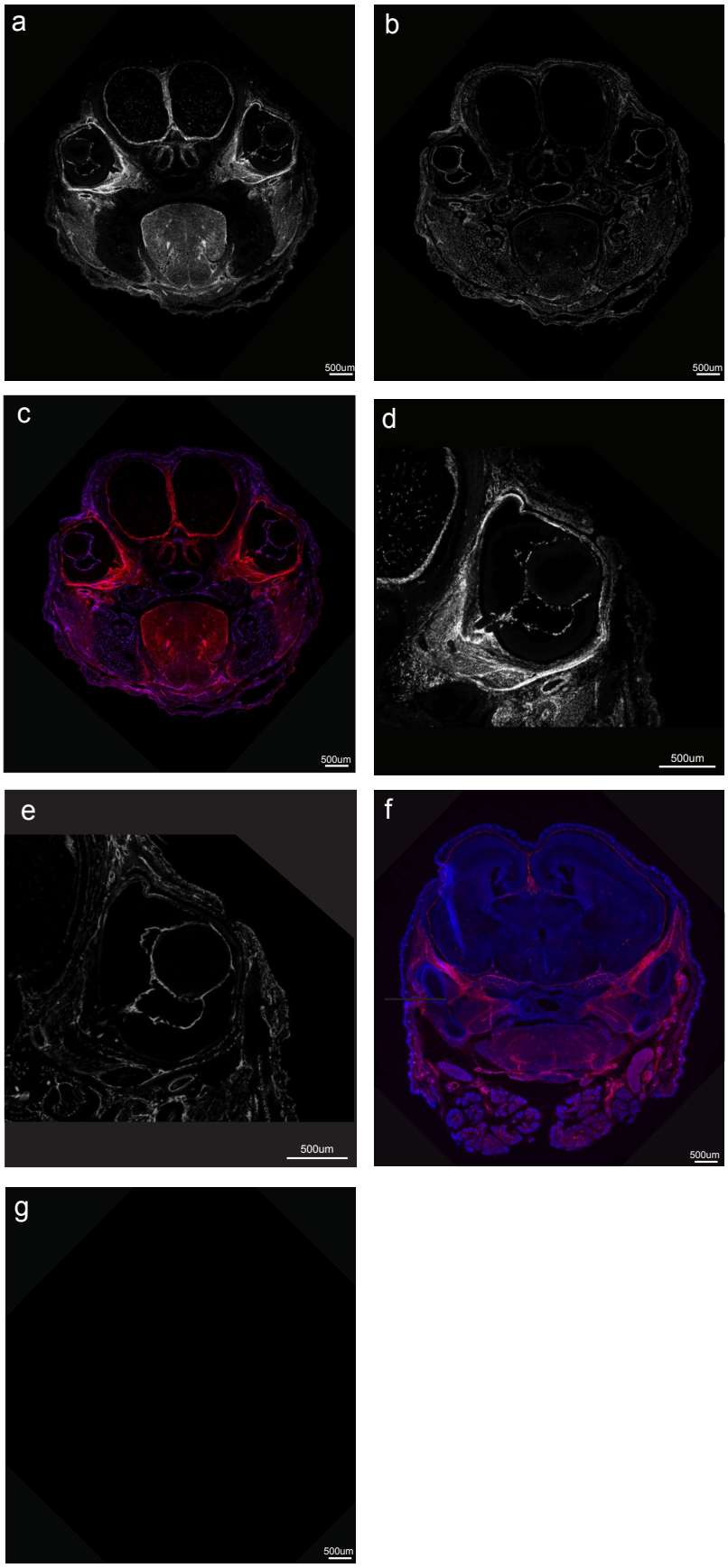
a
500um
b
500um
c
500um
d
500um
e
500um
f
500um
g
500um

**Figure 3.12 Epi-fluorescence imaging of endothelial cell marker CD31 in coronal sections of E18.5 embryos.** A population of tdTomato$^{+}$ cells is perivascular in nature, lining vessels within the head: **(a)** tdTomato alone, **(b)** CD31 alone, **(c)** tdTomato-CD31 overlay, **(d)** tdTomato alone: close-up of the eye from (a), **(e)** CD31 alone: close-up of the eye from (b), **(f, g)** control: no primary antibody applied. Red- tdTomato, Purple- CD31 (Alexa Fluor 647). Scale bars: **(a-g)** = 500μm.

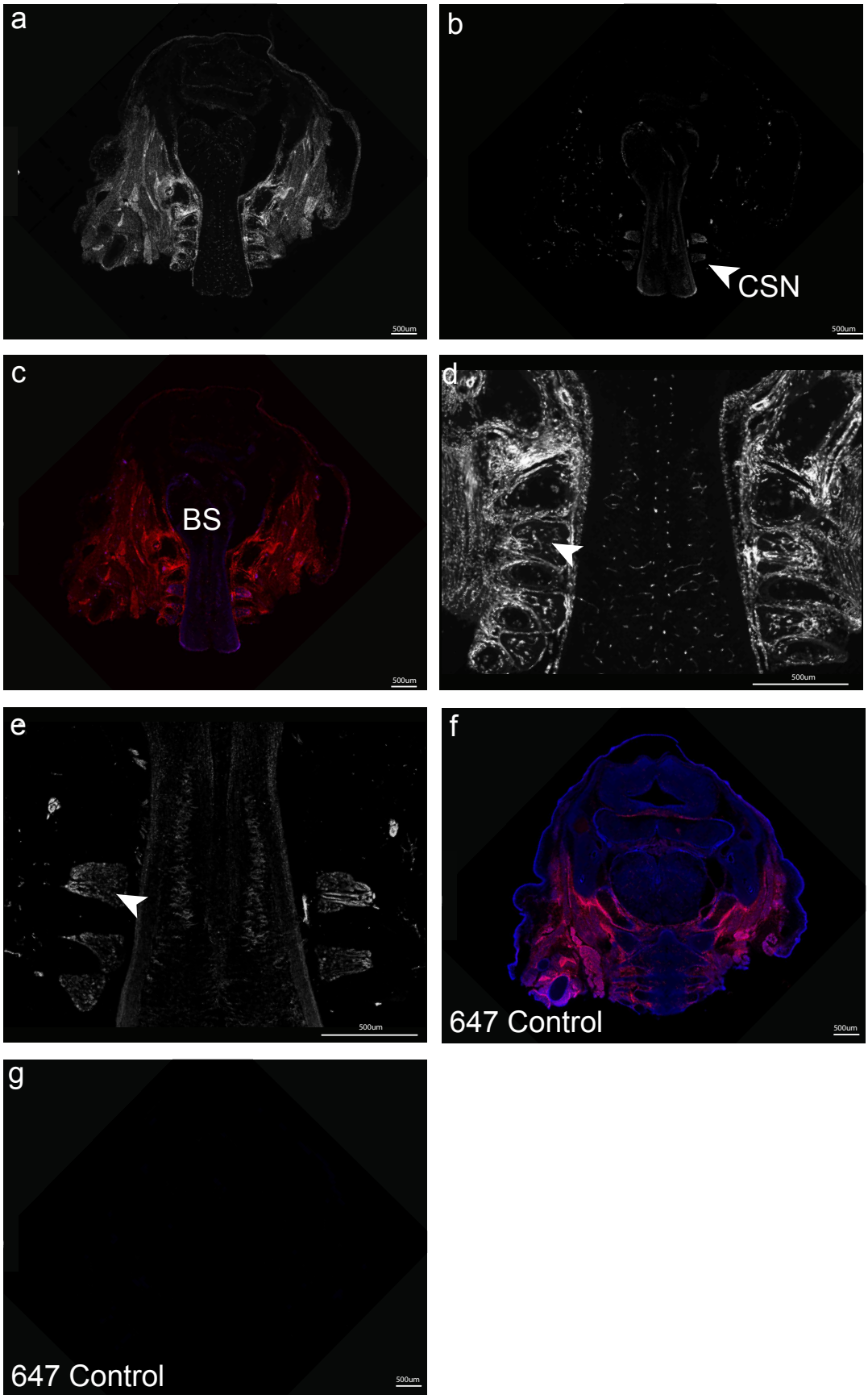
a
500um
b
CSN
500um
c
BS
500um
d
500um
e
500um
f
647 Control
500um
g
647 Control
500um

**Figure 3.13 Epi-fluorescence imaging of neurofilament, a neuron-specific intermediate filament.** Coronal sections are of an embryo with TAM administered at E10, and collected at E16.5. tdTomato$^{+}$ cells are located around neurons, within the brain, cervical spinal nerves (CSN; indicated with arrows), brainstem (BS), and spinal cord. **(a)** tdTomato alone, **(b)** NFH alone, **(c)** tdTomato and NFH overlay, **(d)** tdTomato alone: magnified view of brainstem and cervical spinal nerves, **(e)** NFH alone: magnified view of the area corresponding to (d). **(f, g)** Controls have no primary antibody present. Purple- NFH (Alexa Fluor 647), Blue- nuclei (DAPI), Red- tdTomato. Scale bars: **(a-g)** = 500μm.

### 3.4 Micromass cultures

TAM was administered to pregnant dams at E10 days and embryos were collected at E11.5 days. Cells were isolated from the maxillary, mandibular and frontonasal processes, and were combined together for this experiment. Cartilage nodules were apparent in the micromass cultures of the cells harvested from the facial prominences by days 2-3, upon inspection under light microscopy. In order to confirm the presence or absence of cartilaginous nodules in the micromass cultures under the different conditions, Alcian blue was applied. This stains the cartilage blue under light microscopy. The EC23 condition (synthetic retinoid) exhibited no cartilage nodules, the control exhibited some, AGN 194310 (retinoid acid receptor inverse agonist) demonstrated more, and the BMP4 condition yielded the most.

Next, fluorescent microscopy was applied in order to visualize the tdTomato$^{+}$ cells in relation to the cartilage nodules, since the tdTomato reporter can be detected under fluorescence. When COL2A1 was used to stain type II collagen to demonstrate the cartilaginous nodules under fluorescence, the same relationship between the conditions and the presence of nodules existed, with EC23 demonstrating no nodules, and BMP4 showing the most. The tdTomato$^{+}$ cells were present in all four conditions, and where nodules existed, the tdTomato$^{+}$ cells tended to localize within the area surrounding the nodules rather than within the nodules. Few tdTomato$^{+}$ cells were seen within or overlying the nodules.

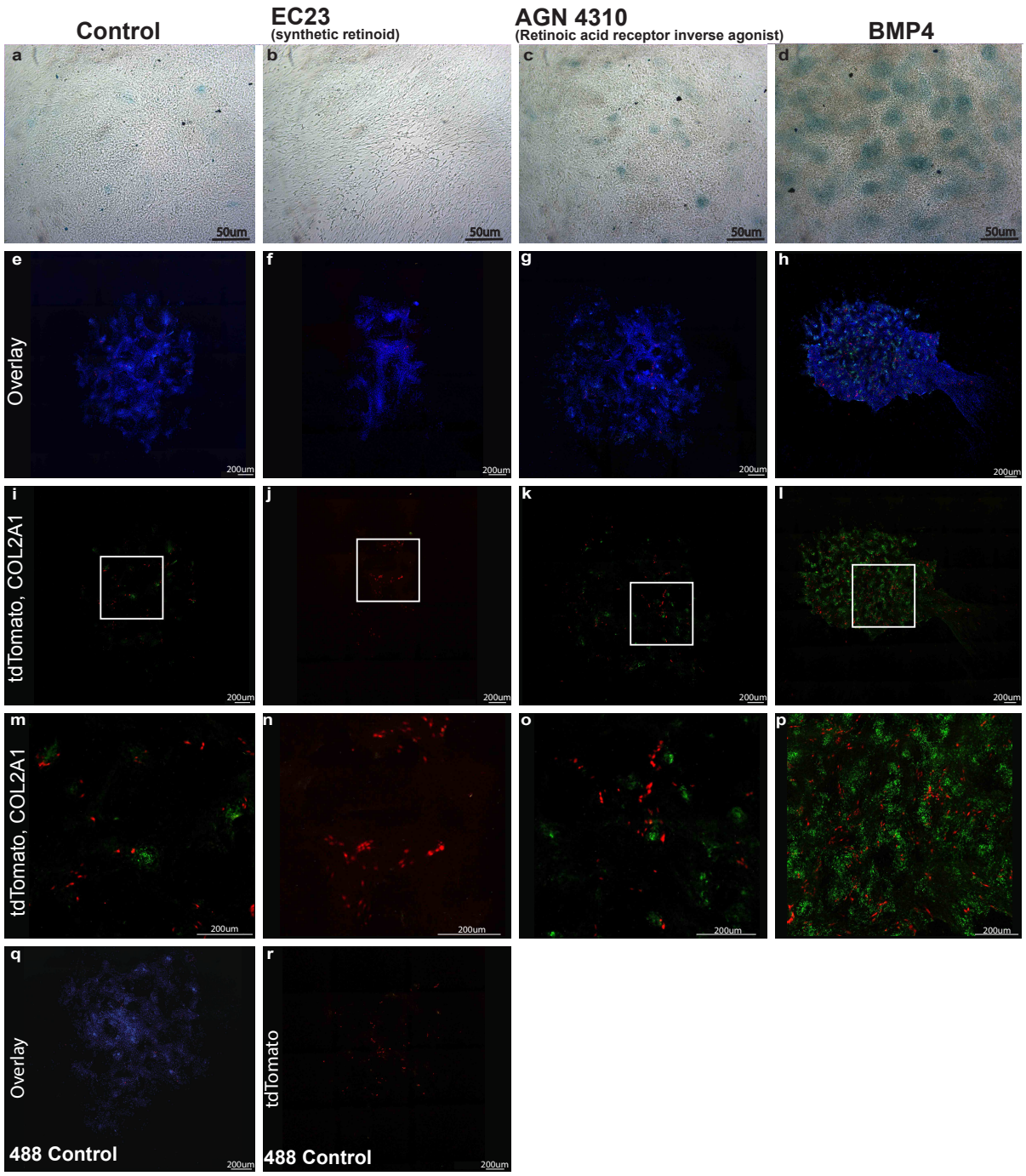


**Figure 3.14 Micromass cultures of the combined maxillary, mandibular and frontonasal processes.** Cultures were seeded at t=0, media was added at t=1.5hrs, and treatments- 95% ethanol for control, EC23, AGN 194310, or BMP4- commenced 24 hours post-seeding, with n=3 samples per condition. Cultures were re-treated at t=3 days, and were fixed at t=4 days.

Alcian blue staining **(a-d)** was performed with 4:1 0.2M HCl:0.5% Alcian blue. Fluorescent imaging of micromass cultures **(e-p):** Red-tdTomato, Blue- nuclei (DAPI), Green- COL2A1 (Alexa Fluor 488). Images **(m-p)** are enlarged from the boxes indicated in **(i-l)**. No primary antibody for CO2A1 was applied to the controls **(q-r).** Scale bars: **(a-d)** = 50μm, **(e-r)** = 500μm.

### 3.5 Single-cell RNA sequencing of cells positive and negative for *Hic1*-expression in the head at E11.5

TAM was administered to pregnant dams at E10 days, and mouse embryos were isolated at E11.5 days. 19 mouse embryo heads were surgically separated from the rest of the body below the mandible, and cells from the head were isolated and sorted into 2 populations using FACS: tdTomato$^+$ (*Hic1*$^+$) cells and tdTomato$^-$ (*Hic1*$^-$) cells. Purified tdTomato$^-$ and tdTomato$^+$ samples were visually evaluated for quality control. Using scRNA-seq, the transcriptome of each cell was determined, and 3,656 cells were sequenced. The following gene markers were analyzed in both the *Hic1*$^+$ and *Hic1*$^-$ populations: regulator of G protein signalling 5 (*Rgs5*) and cluster of differentiation 146 (*Cd146*) for perivascular markers, SRY-box 9 (*Sox9*) as a neural crest-associated marker, dentin matrix acidic phosphoprotein 1 (*Dmp1*) for an odontogenic marker, forkhead box A2 (*Foxa2*) and eomesodermin (*Eomes*) for mesodermal markers, desmin (*Des*) as a muscle-associated marker and type II collagen (*Col2a1*) for a cartilage-expressed marker. Plots were generated using K-means clustering on Loupe Cell Browser (10X Genomics) and were assessed visually for the presence or absence of gene expression, and for specific clusters of cells generating signals. Each dot on the plot represents a single cell, and the presence of colour indicates the presence of a specific kind of RNA transcript in that cell.

From this cluster analysis, it was determined that the *Hic1*$^+$ cells represent multiple mesenchymal populations including a distinct perivascular population marked by *Rgs5* and *Cd146* that was absent from the *Hic1*$^-$ cells. Furthermore, a distinct odontogenic population marked by *Dmp1* was present in the *Hic1*$^+$ cells but absent from the *Hic1*$^-$ cells. Neural crest-associated and cartilage-associated marker *Sox9* was present in both the *Hic1*$^+$ and *Hic1*$^-$

groups of cells. Mesodermal markers *Foxa2 and Eomes* were absent from the *Hic1*$^{+}$ cells, but were present in the *Hic1*$^{-}$ cells. The muscle-associated intermediate filament *Des* was present in both the *Hic1*$^{+}$ and *Hic1*$^{-}$ groups of cells, as was the cartilage-expressed marker *Col2a1*.

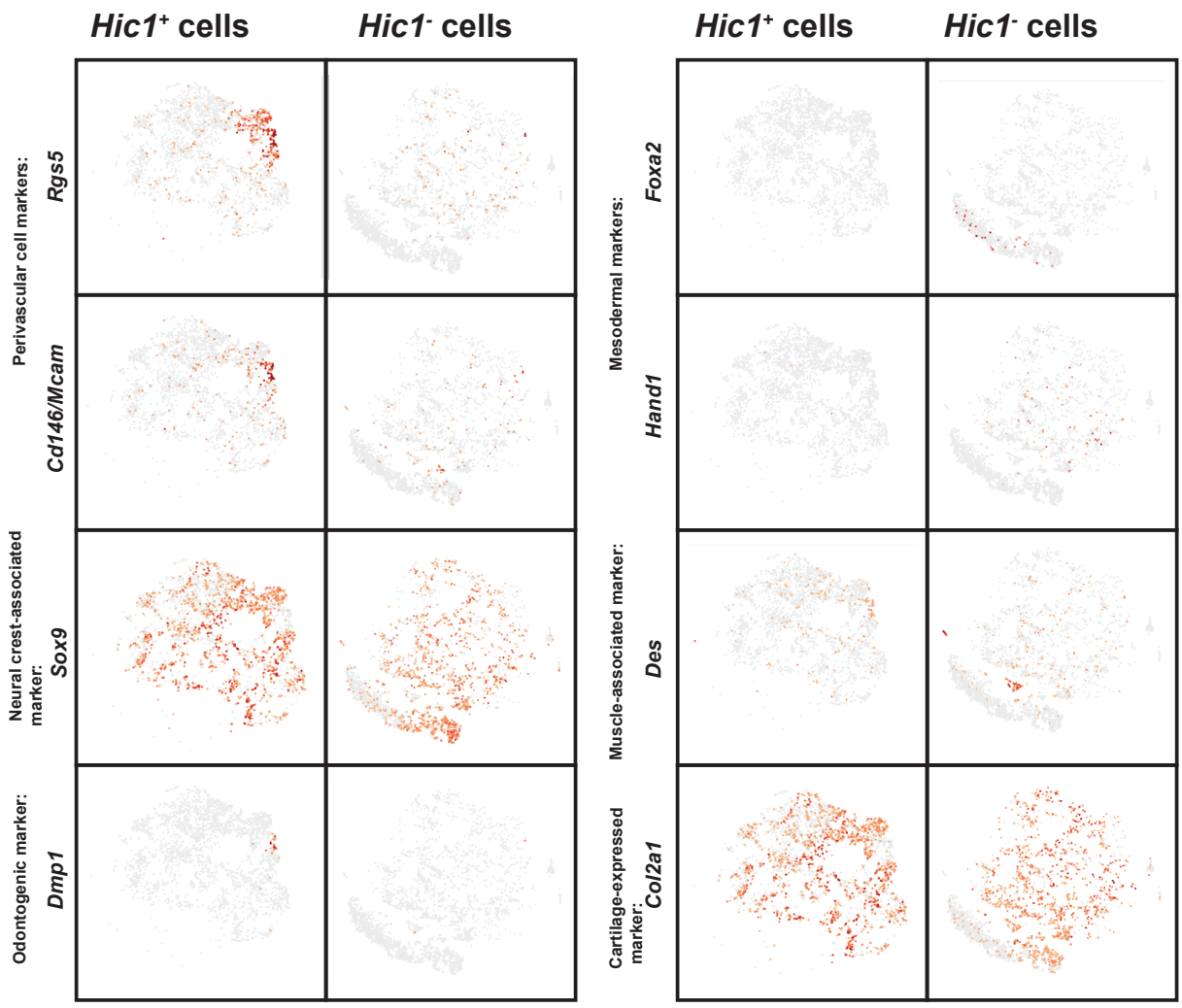


**Figure 3.15 scRNA-seq performed on *Hic1*$^{+}$ and *Hic1*$^{-}$ cells derived from the head.** These two populations of cells were isolated with FACS at E11.5 days, with TAM administered at E10 days. Each dot represents a single cell, and the presence of colour represents the presence of RNA at E11.5. The endothelial markers *Rgs5 and Cd146* are present in a distinct perivascular population in the *Hic1*$^{+}$ cells, and are absent from the *Hic1*$^{-}$

cells of the head. Neural crest-associated and cartilage-expressed marker *Sox9* is present in both the *Hic1*$^{+}$ and *Hic1*$^{-}$ populations. Odontogenic/osteogenic marker *Dmp1* is present in a discrete population of cells in the *Hic1*$^{+}$ head, but is absent from the *Hic1*$^{-}$ head. Mesodermal markers *Foxa2* and *Eomes* are absent from the *Hic1*$^{+}$ cells, but are present in the *Hic1*$^{-}$ cells. The muscle-associated intermediate filament *Des* is present in both the *Hic1*$^{+}$ and *Hic1*$^{-}$ populations, as is the cartilage-expressed marker *Col2a1*.

# CHAPTER 4 – DISCUSSION

## 4.1 Lineage tracing analysis of *Hic1*-expressing cells

### 4.1.1 Timing

Since considerable migration of NCCs has been found to occur during the period of E8.5-E10.5 (Kubota et al., 1996), TAM was administered at E8.5, E9.5 (Figure 3.1 and 3.2) and E10 (Figures 3.3-3.9) in order to assess the onset of *Hic1* expression. From Figure 3.1, it appeared that E8.5 preceded the onset of *Hic1* expression, as no tdTomato reporter marking *Hic1*$^+$ cells was present. The limited fluorescence present was attributed to the autofluorescence of blood at this stage. At E9.5, cells began to emerge from the posterior aspect of the head, in a region consistent with where CNCCs originate off of the neural crest. This time-point is later than the time at which CNCCs begin to stream ventrolaterally from the dorsal aspect of the neural tube, around 21 days in humans and around the 4-somite stage (~8 days) in mice (Sperber et al., 2010) (Huang and Thesleff, 2013) (Nichols, 1981). The timing and location of emergence suggests that *Hic1*-expressing cells represent a population of NCC-derived cells or similar, rather than a population of NCCs. Due to the limited numbers of cells labelled at E13.5 in the embryos administered TAM at E9.5, future embryos on which lineage tracing was performed were administered TAM at E10.

### 4.1.2 Localization of the cellular fate of *Hic1*-expressing cells

In the lineage tracing analysis of *Hic1*-expressing cells, every structure in which *Hic1*$^+$ cells were present was CNCC-derived (Table 1). tdTomato$^+$ cells were seen in the meninges, spinal nerves, ganglia, the cartilaginous nasal septum and nasal connective tissues, connective tissue elements within the masticatory muscles and muscles of facial expression, in

perivascular cell populations surrounding vessel walls, in perineural cell populations including those around the optic nerves, in the stroma of the salivary glands, in and around the pituitary gland, in the cornea and hyaloid cavity of the eye, in tissue adjacent to the semicircular canals of the inner ear, as well as in the developing dental papilla/pulp, and the periodontal ligament. All of the structures noted are of known NCC origin, supporting the hypothesis that the *Hic1*-expressing cells represent a population of CNC-derived cells.

*Hic1*$^{+}$ cells were abundant within the muscular compartment. The myogenic cells of muscle are mesodermally derived; however, the surrounding muscular connective tissue and tendons are CNCC-derived, making it plausible for a population of CNCC derivatives to be present within the developing muscles (Grenier et al., 2009).

*Hic1*$^{+}$ cells were present in chondrocytes, which is shown morphologically (Figure 3.10) by means of SOX9 staining (Figure 3.11), and via scRNA-seq for *Col2a1* (Figure 3.15). The *Hic1*$^{+}$ cells were highly concentrated around the nose throughout development, the nose having many cartilaginous components.

Another reason for the abundance of *Hic1*$^{+}$ cells in the nasal structures is that *Hic1*$^{+}$cells are perivascular in nature. Immunohistochemistry staining co-localized tdTomato$^{+}$ cells with the endothelial cell marker CD31 (Figures 3.11, 3.12), demonstrating the presence of a perivascular population. The scRNA-seq (discussed later) also identified a perivascular cell population among the *Hic1*$^{+}$ cells (Figure 3.15). The connective tissue of the nose is highly vascularized in order to filter, heat and humidify air, and to provide fluid and oxygen transport (Ince et al., 2012). *Hic1*$^{+}$ cells may contribute to the perivascular populations of cells here. Given the high vascularity around the pituitary gland, and the hyaloid cavity of the eye, the presence of *Hic1*$^{+}$ cells seen in the lineage tracing analysis is understandable.

Staining for the neuron-specific intermediate filament NFH (Figure 3.13) showed that *Hic1*$^+$ cells were present within the brain, brainstem, cervical spinal nerves and spinal cord; however, the *Hic1*$^+$ cells were not co-localized with the NFH$^+$ cells; rather, they were located around the neurons. The trigeminal ganglia also had a strong tdTomato$^+$ signal (Figures 3.4, 3.8, 3.9). From immunohistochemistry staining, we confirmed the presence of *Hic1*$^+$ cells in perivascular, perineural and cartilaginous tissues. The *Hic1*$^+$ cells contribute to various mesenchymal tissues in the developing head.

The structures in which *Hic1*$^+$ cells were identified during the lineage tracing analysis performed here, directly coincide with some, but not all of the phenotypic features demonstrated in the *Hic1* knockout mouse studied by Carter *et al*. The missing and underdeveloped eyes in the *Hic1* knockout mouse correspond with the presence of tdTomato$^+$ cells in the eyes, and the abnormal ear development may relate to the presence of tdTomato$^+$ cells outside of the semicircular canals. tdTomato$^+$ cells around the external ears were not apparent at the time points investigated. The overall underdevelopment of these knockout mice may relate to the presence of tdTomato$^+$ cells in and around the pituitary gland. Knockout mice showed acrania and exencephaly, and although tdTomato$^+$ signal was present within the brain and overlying meninges, it was not evident within the bones of the cranial vault (Carter et al., 2000). Perhaps the developmental abnormalities seen in the dura mater and the brain in the *Hic1* knockout mouse have negative secondary effects on the development of the skull vault. The presence of tdTomato$^+$ cells within the brain correlates well with the smooth-surface malformation (lissencephaly) and bitemporal narrowing seen in patients with MDS (Allanson et al., 1998).

Interestingly, *Hic1*$^{+}$ cells were not evident within Meckel's cartilage, which is derived from CNCCs, according to *Wnt1* lineage tracing analysis (Chai et al., 2000). *Hic1*$^{+}$ cells were also absent from the anterior and posterior cranial base, the majority of the hyoid bone, and the incus and stapes. The absence of *Hic1*$^{+}$ cells from these cartilaginous/cartilaginous-derived structures can be interpreted in two ways. Firstly, *Hic1* may be expressed in a specific population of NCC derivatives, but may not be present in all NCC derivatives. This concept is supported by the scRNA-seq that demonstrated that the NCC-associated marker *Sox9* was expressed in both the tdTomato$^{+}$ and tdTomato$^{-}$ populations. A second reason for the absence of *Hic1* from some of the known CNCC-derived structures has to do with the time at which reporter-expression was induced. The TAM in these experiments was administered at E10 days, but it is possible that *Hic1* expression persists, and that it is the cells that begin expressing *Hic1* after E10 that contribute to the CNCC-derived structures where *Hic1* was not seen (i.e. Meckel's cartilage). From the lineage tracing analysis performed in this study, it was evident that embryos with TAM administration at E8.5 and E9.5 did not demonstrate the same tdTomato expression profile as the embryos with TAM administration at E10. This affirms the possibility that a different tdTomato expression profile may be seen with administration of TAM at later developmental time points.

### 4.1.3 A role for *Hic1* in cleft palate

The palatal clefting phenotype evident in Carter's study of the *Hic1* knockout is a craniofacial anomaly of particular interest in the field of orthodontics, because cleft palate represents a condition commonly requiring orthodontic treatment. From our lineage tracing analysis in this study (Figures 3.2-3.13), it was evident that *Hic1*$^{+}$ cells were not present in the developing palatal shelves of the secondary palate, nor in the primary palate, implying that the

underlying cause for the cleft likely originated outside of these structures. One hypothesis for this clefting involves the abundance of *Hic1*$^{+}$ cells within the tongue. *Hic1* encodes for a tumor suppressor, that when mutated, would likely result in increased cellular proliferation. If there was an increase in proliferation in the tongue, the tongue may be unable to descend, and this could prevent the palatal shelves from reorienting from a vertical to a horizontal position, allowing them to approximate and fuse (Ferguson, 1988) (Huang and Thesleff, 2013). A second hypothesis involves the concentration of *Hic1*$^{+}$ cells in the nasal region. If a mutation of *Hic1* results in increased proliferation of the nasal tissues, then it may be possible that this proliferation prevents the shelves from meeting and fusing. Also, the nasal septum could proliferate to such a great extent that it interferes with the union of the palatal processes. A third reason could involve changes to cellular signalling pathways, initiated by the reduction of *Hic1* activity in the knockout, that could have downstream effects on the formation of the palate.

It should be noted that the holoprosencephaly seen in the *Hic1* knockout mice, characterized by a fused eyespot and protruding telencephalon, is a classic presentation of the *Shh* knockout mouse. The SHH signalling pathway is extremely important in craniofacial development, and specifically, in the development of the lip and palate (Cox, 2004). For example, it has been demonstrated that SHH blocking antibodies administrated to chick faces before fusion resulted in bilateral cleft lip/palate (Hu and Helms, 1999). Perhaps future studies could aim to analyze the cell signalling pathways downstream of *Hic1* to improve understanding of the role of *Hic1* and the effects of a loss of *Hic1* on craniofacial development. *Shh* represents one candidate marker to study.

### 4.1.4 *Hic1*$^+$ cells and tooth development

In the lineage tracing analysis, *Hic1*$^+$cells were present within the dental papilla/pulp of the developing tooth, and in the cells surrounding the tooth that will likely become the periodontal ligament. *Hic1*$^+$cells were mainly seen at the later developmental time-points (i.e. E20.5) and were not seen in the earlier time-points that included the initiation, bud or cap stages. Work by Chai previously identified *Wnt1*$^+$ CNCCs in the condensed dental mesenchyme, the dental papilla, odontoblasts, dentine matrix, pulp, cementum and periodontal ligament (Chai et al., 2000). Given that NCC derivatives represent a population of mesenchymal progenitors, it is possible that the *Hic1*$^+$cells present within and around the developing teeth represent dental mesenchymal stem cells. There are 5 main types of these cells: dental pulp stem cells (DPSCs), periodontal ligament stem cells (PDLSCs), stem cells from apical papilla (SCAP), dental follicle progenitor cells, and stem cells from exfoliated deciduous teeth (SHED) (Achilleos and Trainor, 2012) (Huang et al., 2009). Dental pulp stem cells (DPSCs) were previously determined to exist within a perivascular niche residing in the pulp (Arthur et al., 2008). Since our experiments demonstrated CD31-positive staining of *Hic1*$^+$ cells, and since scRNA-seq identified a distinct perivascular population of cells in the *Hic1*$^+$ heads using markers *Cd146* and *Rgs5*, it is possible that the *Hic1*$^+$cells represent future DPSCs.

## 4.2 *Hic1*$^+$ cells and cartilage

After seeing the abundance of *Hic1*$^+$cells in and around the developing nasal capsule and turbinates in the lineage tracing analysis, we sought to further investigate the relationship between *Hic1*$^+$cells and cartilage formation. We applied a micromass technique, where cells isolated and pooled from the maxillary, mandibular and frontonasal processes at E11.5 were

grown in high-density cultures. Factors were applied that were known to stimulate (BMP4) or inhibit (retinoid acid) chondrogenesis (Miljkovic et al., 2008) (Underhill and Weston, 1998). From our micromass cultures, we saw that tdTomato$^{+}$ cells were more concentrated around the cartilaginous nodules rather than within the nodules, mimicking the pattern of distribution of *Hic1*-expressing cells present in the nasal structures. In the nasal structures, *Hic1*$^{+}$ cells were more abundant in the connective tissue surrounding the nasal cartilage than in the nasal cartilage. *Hic1*$^{+}$ cells did give rise to some cartilage nodules in micromass culture, a finding that is consistent with the presence of *Hic1*$^{+}$ cells and/or their progeny within cartilaginous structures in the developing head, particularly in the nasal cartilage (Figure 3.10). The *Hic1*$^{+}$cells persisted around the nasal areas long after the cartilage was deposited, suggesting a role for these cells in the maintenance and secondary remodeling of the nasal cartilage. This may also be a potential reason for the presence of *Hic1*$^{+}$cells around the basioccipital bone, which is mesodermally derived (McBratney-Owen et al., 2008). The *Hic1*$^{+}$cells may be recruited to help with maintenance/remodeling of cartilage.

Previously, Ralphs applied high density micromass culture techniques to cells derived from the facial primordia of mice- specifically the frontonasal mass mesenchyme, the maxillary mesenchyme and the mandibular mesenchyme (Ralphs, 1992). He found that cartilaginous nodules formed after 3 days of culture in the frontonasal and maxillary mesenchyme, but not in the mandibular mesenchyme (Ralphs, 1992). This is consistent with our cultures, which demonstrated cartilaginous nodules by days 2-3. Furthermore, the cells Ralphs cultured were isolated at E11, E11.5, E12, E12.5, E13, E13.5 and E14, and the chondrogenesis occurred in the frontonasal mass only for cells isolated between E11.5 and E13, while in the maxillae, chondrogenesis only occurred at E12.5 (Ralphs, 1992). Finally,

most of the chondrogenesis was found to occur in the frontonasal mass, rather than in the maxillae (Ralphs, 1992). Based on these findings, we may be able to attribute most of the chondrogenesis in our study to the cells isolated from the frontonasal prominence.

### 4.3 Single-cell RNA sequencing

scRNA-seq was performed in order to compare the gene expression of cells positive and negative for *Hic1* expression. The tdTomato-reporter was induced at E10, and the cells were collected from embryos at E11.5, meaning the *Hic1*$^{+}$ population would include cells expressing *Hic1* at E10, and the descendants of these cells.

As previously mentioned, many of the structures to which *Hic1*$^{+}$ cells contributed in the lineage tracing analysis were NCC-derived. Furthermore, the location from which the *Hic1*$^{+}$ cells originated, near the neural tube at the dorsal aspect of the head, would also suggest that the *Hic1*$^{+}$cells represent a population of CNCC derivatives. scRNA-seq allowed us to further assess the nature of this population. Firstly, *Foxa2* and *Eomes*, which are recognized as mesodermal markers, were absent from the *Hic1*$^{+}$ population, but were present in the *Hic1*$^{-}$ population (Poh et al., 2014) (Russ et al., 2000). The absence of expression of these 2 genes in the *Hic1*$^{+}$ cells suggests that *Hic1*$^{+}$ cells do not give rise to mesodermal structures, a finding which would be expected if the *Hic1*$^{+}$ cells represent a NCC-derived population, as these cell types are mutually exclusive. From scRNA-seq, *Hic1*$^{+}$ cells were shown to express *Col2a1*, a marker for cartilage, and *Sox9*, a transcription factor required for the initiation and maintenance of chondrogenesis (Bi et al., 1999) (Wright et al., 1995). *Sox9* has been identified as a known marker of neural crest progenitors (Jiang et al., 2009) (Achilleos and Trainor, 2012). *Hic1*$^{+}$ cells also stained positive for SOX9 in the nasal and vertebral cartilages (Figure 3.11), confirming the chondrogenic fate of *Hic1*$^{+}$ cells. This

supports our hypothesis that *Hic1*$^{+}$ cells represent a population of CNC-derived cells that contribute to the formation of craniofacial mesenchyme. It should be noted that *Sox9* was present in both the *Hic1*$^{+}$ and *Hic1*$^{-}$ populations in the scRNA-seq. This supports the notion that the *Hic1*$^{+}$ population is unlikely to include all CNCC derivatives, given the presence of *Sox9* in the *Hic1*$^{-}$ population. This corresponds with what was seen in the lineage tracing analysis, as tissues known to be NCC-derived: Meckel's cartilage, the palate, and the mandible, for example, were negative for *Hic1* expression. *Hic1*$^{+}$ cells may therefore represent a distinct subpopulation of CNCC derivatives. The possibility of the existence of CNCC subpopulations was also mentioned by Chai *et al* in the lineage tracing analysis of the *Wnt1*$^{+}$ CNCC population (Chai et al., 2000).

A distinct population of cells expressing *Dmp1* was present in the tdTomato$^{+}$ head, but absent from the tdTomato$^{-}$ head. *Dmp1* is expressed by odontoblasts and pulpal cells, and encodes for an extracellular matrix protein involved in dentin mineralization and odontogenesis (Lu et al., 2007). Although it is likely that *Dmp1* is expressed by odontogenic or pulpal cells in the mouse embryos, this is not definitive because *Dmp1* has been shown to also exist in bone and cartilage (Feng et al., 2002). The presence of tdTomato$^{+}$ cells in the pulpal and periodontal ligament regions (Figure 3.13) offers support for the view that *Dmp1*-tdTomato$^{+}$ population could contribute to the developing teeth, and may represent dental pulp stem cells (Achilleos and Trainor, 2012) (Arthur et al., 2008).

## 4.4 Conclusion and overall significance

From lineage tracing analysis, *Hic1*$^{+}$ cells and/or their progeny give rise to mesenchyme within facial/masticatory muscles, tendons, tongue, meninges, nasal cartilage/ connective tissue, eyes, salivary gland stroma, teeth (dental papilla/pulp/periodontal

ligament), and to populations of perivascular and perineural cells, including those within the brain. *Hic1* is not seen within the palatal shelves, Meckel's cartilage, or the developing cranial base. The localization of *Hic1*$^{+}$ cells around nasal cartilage in the lineage tracing analysis histology and in the micromass cultures of cartilaginous nodules suggests that *Hic1*$^{+}$ cells have a role in cartilage remodeling. Finally, scRNA-seq suggests *Hic1*-expressing cells may be of NCC origin or similar, and represent mesenchymal progenitors, giving rise to various tissue types, including populations of perivascular cells, muscle, cartilage, and teeth and/or bone tissues. ***From this study, we can conclude that Hic1-expressing cells contribute to various mesenchymal tissues during craniofacial development, and likely represent a population of cranial neural crest-derived cells.***

Understanding the nature of this population of cells may be important in future regenerative medicine, as *Hic1*-expressing cells have the ability to give rise to various tissue types. Harnessing the differentiation-potential of these cells could be of use in a range of therapeutics from tissue regeneration to stem cell therapies. As well, the lineage tracing model employed here deepens our understanding of the contribution of *Hic1* in craniofacial development and highlights areas for future inquiry. For example, the absence of *Hic1*$^{+}$ cells from the palatal shelves, when the *Hic1* knockout mice exhibit clefting, may lead to future investigations uncovering new mechanisms responsible for orofacial clefting and may provide a better understanding of the molecular signaling involved.

## 4.5 Strengths and limitations

The main strength of this study is the robust method of indelible lineage tracing used, that allowed us to induce tdTomato reporter expression at the onset of *Hic1* expression and track the population of *Hic1*-expressing cells and descendants throughout embryonic

development with a pulse-chase approach. This technique eliminates false positive and false-negative signals frequently seen in immunohistochemical staining for a protein. A weakness with our lineage tracing strategy was that most of the tracing involved TAM administration at E10, preventing us from tracking populations/derivatives of cells with a later onset of *Hic1* expression. This limitation could be overcome by inducing tdTomato reporter expression at later time points. Such an approach was taken in the lineage tracing that followed the cellular fate of *Msx2*-expressing mesenchymal cells with reporter induction occurring at: E10.5 E11.5, E13.5, E17.5 (Sakagami et al., 2018).

The cryosections used for lineage tracing analysis work well in that they preserve the native fluorescent tdTomato signal; however, they only provide a 2-dimensional picture. 3-dimensional imaging on a confocal microscope, with optical projection tomography or live embryo imaging could be a better way to view the migratory pattern of the *Hic1*-expressing cells in the embryos. As well, the cryosections varied in thicknesses within and between samples, ranging from 10-30μm. This may be responsible for some of the variability seen between samples at the same time-point, as more tdTomato$^{+}$ cells may have been evident in thicker sections. Variability can also be attributed to the precision of the timing of the vaginal plug that would affect the time period the TAM was active for.

The micromass culture experiments allowed us to examine the relationship of the *Hic1*-expressing cells relative to the cartilaginous nodules. A limitation of our study was that the mandibular, maxillary and frontonasal prominences- specifically the mesial nasal process- were pooled in order to increase the number of cells for micromass cultures, as only 11 embryos were available for this procedure. This prevented us from being able to identify which of the facial prominences in our study had *Hic1*$^{+}$ cells contributing to cartilage

formation. Still, given the findings of Ralphs, one would suspect that the cartilaginous nodules formed from our pooled frontonasal, maxillary and mandibular processes isolated at E11.5 were likely derived predominately from the frontonasal mass (Ralphs, 1992). As well, in the lineage tracing analysis results, few, if any tdTomato$^{+}$ cells were seen in the maxilla or mandible compared to in the nasal region, a finding which also supports the frontonasal origin of the cartilage-forming *Hic1*$^{+}$ cells. A second limitation pertaining to the micromass experiments was that the number of tdTomato$^{+}$ cells could not be quantified in the different conditions, since the chamber slides occasionally lost regions of the sample during the processing for immunofluorescent COL2A1 staining, and adjusting the fixation time did not improve this. One may have expected more tdTomato$^{+}$ cells in the BMP4 condition, due to increased proliferation of the nodules/surrounding connective tissue.

scRNA-seq allowed us to assess the expression profile of individual *Hic1*$^{+}$ and *Hic1*$^{-}$ cells. It also identified specific populations of cells (i.e. perivascular, odontogenic). scRNA-seq provides an assessment of cell heterogeneity, since it captures the transcriptome of each individual cell, rather than presenting data as a population average, the way a classical biochemical assay such as a Western blot would (Hoppe et al., 2014). A weakness with this method is that transcripts of low abundance may be undetected. Another limitation of scRNA-seq data is that the presence of a transcript within the transcriptome does not necessarily mean that the corresponding protein is expressed. Since NCC and many of their derivatives are multipotent in nature, scRNA-seq provided us with insight as to what a cell can potentially signal for or differentiate into; however, this does not confirm that it will. The fate of CNCCs is not only determined by genetics, but also by the environment surrounding the cells. This was demonstrated by the original CNCC chimera studies. As well, conclusions

drawn from scRNA-seq data were based on visual assessment of the presence or absence of signals on plots generated by Loupe Cell Browser (10X Genomics) using K-means clustering. No effort was made to create plots to quantify the data to make comparisons. Although we were able to apply this data to characterize the *Hic1*$^{+}$ and *Hic1*$^{-}$ cells, the analysis rendered limits the conclusions that can be made regarding the scRNA-seq data.

## 4.6 Future direction

In order to investigate further the cause of the palatal clefting that results in the *Hic1* knockout mouse, it would be ideal to apply a conditional gene knockout. For example, the knocking out of the *Hic1* gene could be restricted to the tongue, and craniofacial structures could be assessed in order to determine if there is increased proliferation of the tongue that results in facial clefting. *Hic1* could be conditionally knocked out of the nasal cartilage as well, in order to understand the developmental consequences of this. Unfortunately, there are no known genes expressed at E10 that are exclusive to the tongue or to the nasal cartilage, preventing this from being performed in future studies.

Previous characterization of the *Hic1* knockout mouse was performed with light microscopy and assessment of gross specimens (Carter et al., 2000). A more thorough investigation of the knockout phenotype could be performed with use of micro-computed tomography and micro-magnetic resonance imaging to better characterize hard tissues and soft tissues respectively, in three dimensions. By comparing the knockouts to the controls, the relative sizes of the nasal structures, the tongue, and more detailed descriptions of the nature of the facial clefts could be obtained. This may provide further insight into the brain and skull abnormalities seen in the knockout mice, and in MDS. The main caveat here is that previous characterization of the *Hic1* knockout demonstrated a wide range of phenotypes, and

a large sample of null-embryos would need to be obtained in order to comprehensively examine the knockout phenotype (Carter et al., 2000).

With regards to tooth development, tdTomato$^+$ cells were present in and around the teeth at the later embryonic time-points (i.e. E20.5), rather than the earlier time-points (initiation, bud, cap). Applying the anti-HIC1 antibody for immunohistochemical staining of mouse embryo heads at various developmental time-points may demonstrate a role for HIC1 that may be independent of NCCs, if *Hic1* expression persists or turns on after the migration of the NCC population. The postnatal tooth development could be studied as well in this manner.

In the future, a more thorough analysis of the scRNA-seq data could be rendered, in order to compare the transcriptome of the *Hic1*$^+$ in the developing head with the *Hic1*$^+$ cells in the rest of the body. Traditionally, the NCCs have been categorized into distinct populations, depending on the axial level of the neural tube from which they are derived. These include cranial, cardiac, vagal and trunk NCCs (Sauka-Spengler and Bronner, 2010). Future comparison of the *Hic1*$^+$ scRNA-seq output may highlight similarities and differences between these populations. Many of the signaling processes in head development are similar to those in limb development, and several craniofacial syndromes present with limb defects, or even require limb defects for a specific diagnosis, including Apert syndrome (OMIM #101200), Saethre-Chotzen syndrome (OMIM #101400) and Pfeiffer syndrome (OMIM #101600) (Wilkie and Morriss-Kay, 2001). The *Hic1* knockout mouse also demonstrated both limb and craniofacial developmental anomalies. scRNA-seq may be a useful tool for comparison of the *Hic1*$^+$ cells in the limbs and *Hic1*$^+$ cells in the head.

Finally, the focus of this project was lineage tracing analysis during prenatal development. Future research could investigate the tissues derived from the *Hic1*$^{+}$ population in the postnatal period.

## REFERENCES


**Achilleos, A. and Trainor, P. A.** (2012). Neural crest stem cells: discovery, properties and potential for therapy. *Cell Research* **22**, 288–304.

**Ahlstrom, J. D. and Erickson, C. A.** (2009). The neural crest epithelial-mesenchymal transition in 4D: a "tail" of multiple non-obligatory cellular mechanisms. *Development* **136**, 1801–1812.

**Allanson, J. E., Ledbetter, D. H. and Dobyns, W. B.** (1998). Classical lissencephaly syndromes: does the face reflect the brain? *J. Med. Genet.* **35**, 920–923.

**Arthur, A., Rychkov, G., Shi, S., Koblar, S. A. and Gronthos, S.** (2008). Adult Human Dental Pulp Stem Cells Differentiate Toward Functionally Active Neurons Under Appropriate Environmental Cues. *Stem Cells* **26**, 1787–1795.

**Baggiolini, A., Varum, S., Mateos, J. M., Bettosini, D., John, N., Bonalli, M., Ziegler, U., Dimou, L., Clevers, H., Furrer, R., et al.** (2015). Premigratory and migratory neural crest cells are multipotent in vivo. *Cell Stem Cell* **16**, 314–322.

**Bi, W., Deng, J. M., Zhang, Z., Behringer, R. R. and de Crombrugghe, B.** (1999). Sox9 is required for cartilage formation. *Nat. Genet.* **22**, 85–89.

**Bush, J. O. and Jiang, R.** (2012). Palatogenesis: morphogenetic and molecular mechanisms of secondary palate development. *Development* **139**, 828–828.

**Carter, M. G., Johns, M. A., Zeng, X. B., Zhou, L., Zink, M. C., Mankowski, J. L., Donovan, D. M. and Baylin, S. B.** (2000). Mice deficient in the candidate tumor suppressor gene Hic1 exhibit developmental defects of structures affected in the Miller-Dieker syndrome. *Hum. Mol. Genet.* **9**, 413–419.

**Chai, Y., Jiang, X., Ito, Y., Bringas, P., Han, J., Rowitch, D. H., Soriano, P., McMahon, A. P. and Sucov, H. M.** (2000). Fate of the mammalian cranial neural crest during tooth and mandibular morphogenesis. *Development* **127**, 1671–1679.

**Chai, Y., Mah, A., Crohin, C., Groff, S., Bringas, P., Le, T., Santos, V. and Slavkin, H. C.** (1994). Specific Transforming Growth Factor-β Subtypes Regulate Embryonic Mouse Meckel's Cartilage and Tooth Development. *Developmental Biology* **162**, 85–103.

**Chiang, C., Ying, L., Lee, E., Young, K. E., Corden, J. L., Westphal, H. and Beachy, P. A.** (1996). Cyclopia and defective axial patterning in mice lacking Sonic hedgehog gene function. *Nature* **383**, 407–413.

**Cohen, A. M.** (1977). Independent expression of the adrenergic phenotype by neural crest cells in vitro. *Proc. Natl. Acad. Sci. U.S.A.* **74**, 2899–2903.

**Couly, G., Grapin-Botton, A., Coltey, P., Ruhin, B. and Le Douarin, N. M.** (1998). Determination of the identity of the derivatives of the cephalic neural crest:

incompatibility between Hox gene expression and lower jaw development. *Development* **125**, 3445–3459.

**Cox, T. C.** (2004). Taking it to the max: The genetic and developmental mechanisms coordinating midfacial morphogenesis and dysmorphology. *Clin. Genet.* **65**, 163–176.

**Creuzet, S., Couly, G., Vincent, C. and Le Douarin, N. M.** (2002). Negative effect of Hox gene expression on the development of the neural crest-derived facial skeleton. *Development* **129**, 4301–4313.

**Diewert, V. M.** (1985). Development of human craniofacial morphology during the late embryonic and early fetal periods. *Am J Orthod* **88**, 64–76.

**Dixon, J., Trainor, P. and Dixon, M. J.** (2007). Treacher Collins syndrome. *Orthod Craniofac Res* **10**, 88–95.

**Dupin, E., Calloni, G. W., Coelho-Aguiar, J. M. and Le Douarin, N. M.** (2018). The issue of the multipotency of the neural crest cells. *Developmental Biology* doi: 10.1016/j.ydbio.2018.03.024.

**Feng, J. Q., Zhang, J. H., Dallas, S. L., Lu, Y. B., Chen, S., Tan, X. Y., Owen, M., Harris, S. E. and Macdougall, M.** (2002). Dentin matrix protein 1, a target molecule for Cbfa1 in bone, is a unique bone marker gene. *J. Bone Miner. Res.* **17**, 1822–1831.

**Ferguson, M.** (1988). Palate Development. *Development* **103**, 41–60.

**Francis-West, P., Ladher, R., Barlow, A. and Graveson, A.** (1998). Signalling interactions during facial development. *Mechanisms of Development* **75**, 3–28.

**Gnecchi, M (Ed).** Mesenchymal stem cells: Methods and protocols, Methods in molecular biology. New York: Springer Science + Business Media, 2016.

**Grenier, J., Teillet, M.-A., Grifone, R., Kelly, R. G. and Duprez, D.** (2009). Relationship between neural crest cells and cranial mesoderm during head muscle development. *PLoS ONE* **4**, e4381.

**Hall, B. K.** (2000). The neural crest as a fourth germ layer and vertebrates as quadroblastic not triploblastic. *Evol. Dev.* **2**, 3–5.

**Hari, L., Miescher, I., Shakhova, O., Suter, U., Chin, L., Taketo, M., Richardson, W. D., Kessaris, N. and Sommer, L.** (2012). Temporal control of neural crest lineage generation by Wnt/β-catenin signaling. *Development* **139**, 2107–2117.

**Herbarth, B., Pingault, V., Bondurand, N., Kuhlbrodt, K., Hermans-Borgmeyer, I., Puliti, A., Lemort, N., Goossens, M. and Wegner, M.** (1998). Mutation of the Sry-related Sox10 gene in Dominant megacolon, a mouse model for human Hirschsprung disease. *Proc. Natl. Acad. Sci. U.S.A.* **95**, 5161–5165.

**Hilliard, S. A., Yu, L., Gu, S. P., Zhang, Z. Y. and Chen, Y. P.** (2005). Regional regulation of palatal growth and patterning along the anterior-posterior axis in mice. *J Anatomy* **207**, 655–667.

**Hirotsune, S., Fleck, M. W., Gambello, M. J., Bix, G. J., Chen, A., Clark, G. D., Ledbetter, D. H., McBain, C. J. and Wynshaw-Boris, A.** (1998). Graded reduction of Pafah1b1 (Lis1) activity results in neuronal migration defects and early embryonic lethality. *Nat. Genet.* **19**, 333–339.

**Hoppe, P. S., Coutu, D. L. and Schroeder, T.** (2014). Single-cell technologies sharpen up mammalian stem cell research. *Nat. Cell Biol.* **16**, 919–927.

**Hu, D. and Helms, J. A.** (1999). The role of sonic hedgehog in normal and abnormal craniofacial morphogenesis. *Development* **126**, 4873–4884.

**Huang, G. T. J., Gronthos, S. and Shi, S.** (2009). Mesenchymal Stem Cells Derived from Dental Tissues vs. Those from Other Sources: Their Biology and Role in Regenerative Medicine. *J. Dent. Res.* **88**, 792–806.

**Huang G. T. J. and Thesleff, I.** Stem cells in craniofacial development and regeneration. Hoboken: Wiley-Blackwell, 2013.

**Ido, A. and Ito, K.** (2006). Expression of chondrogenic potential of mouse trunk neural crest cells by FGF2 treatment. *Dev. Dyn.* **235**, 361–367.

**Ikeya, M., Lee, S. M., Johnson, J. E., McMahon, A. P. and Takada, S.** (1997). Wnt signalling required for expansion of neural crest and CNS progenitors. *Nature* **389**, 966–970.

**Ince, C., van Kuijen, A.-M., Milstein, D. M. J., Yürük, K., Folkow, L. P., Fokkens, W. J. and Blix, A. S.** (2012). Why Rudolph's nose is red: observational study. *BMJ* **345**, e8311–e8311.

**Ito, Y., Yeo, J. Y., Chytil, A., Han, J., Bringas, P., Nakajima, A., Shuler, C. F., Moses, H. L. and Chai, Y.** (2003). Conditional inactivation of Tgfbr2 in cranial neural crest causes cleft palate and calvaria defects. *Development* **130**, 5269–5280.

**Jaisser, F.** (2000). Inducible gene expression and gene modification in transgenic mice. *J. Am. Soc. Nephrol.* **11 Suppl 16**, S95–S100.

**Jiang, X., Gwye, Y., McKeown, S. J., Bronner-Fraser, M., Lutzko, C. and Lawlor, E. R.** (2009). Isolation and characterization of neural crest stem cells derived from in vitro-differentiated human embryonic stem cells. *Stem Cells and Development* **18**, 1059–1070.

**Jiang, X., Iseki, S., Maxson, R. E., Sucov, H. M. and Morriss-Kay, G. M.** (2002). Tissue origins and interactions in the mammalian skull vault. *Developmental Biology* **241**, 106–116.

**John, N., Cinelli, P., Wegner, M. and Sommer, L.** (2011). Transforming Growth Factor β-Mediated Sox10 Suppression Controls Mesenchymal Progenitor Generation in Neural Crest Stem Cells. *Stem Cells* **29**, 689–699.

**Kaufman, M. H.** The atlas of mouse development, Revised edition. London: Elsevier Academic Press, 1994.

**Kubota, Y., Morita, T. and Ito, K.** (1996). New monoclonal antibody (4E9R) identifies mouse neural crest cells. *Dev. Dyn.* **206**, 368–378.

**Le Douarin N. M. and Kalcheim C.** The Neural Crest. Cambridge UK: Cambridge University Press, 1999.

**Le Douarin, N. M., Renaud, D., Teillet, M. A. and LeDouarin, G. H.** (1975). Cholinergic Differentiation of Presumptive Adrenergic Neuroblasts in Interspecific Chimeras After Heterotopic Transplantations. *Proc. Natl. Acad. Sci. U.S.A.* **72**, 728–732.

**Lewis, A. E., Vasudevan, H. N., O'Neill, A. K., Soriano, P. and Bush, J. O.** (2013). The widely used Wnt1-Cre transgene causes developmental phenotypes by ectopic activation of Wnt signaling. *Developmental Biology* **379**, 229–234.

**Lu, Y., Ye, L., Yu, S., Zhang, S., Xie, Y., McKee, M. D., Li, Y. C., Kong, J., Eick, J. D., Dallas, S. L., et al.** (2007). Rescue of odontogenesis in Dmp1-deficient mice by targeted re-expression of DMP1 reveals roles for DMP1 in early odontogenesis and dentin apposition in vivo. *Developmental Biology* **303**, 191–201.

**McBratney-Owen, B., Iseki, S., Bamforth, S. D., Olsen, B. R. and Morriss-Kay, G. M.** (2008). Development and tissue origins of the mammalian cranial base. *Developmental Biology* **322**, 121–132.

**Miljkovic, N. D., Cooper, G. M. and Marra, K. G.** (2008). Chondrogenesis, bone morphogenetic protein-4 and mesenchymal stem cells. *Osteoarthr. Cartil.* **16**, 1121–1130.

**Minoux, M. and Rijli, F. M.** (2010). Molecular mechanisms of cranial neural crest cell migration and patterning in craniofacial development. *Development* **137**, 2605–2621.

**Nakamura, E., Nguyen M. and Mackem, S.** (2006). Kinetics of tamoxifen-regulated Cre activity in mice using a cartilage-specific CreER$^{T}$ to assay temporal activity windows along the proximodistal limb skeleton. *Dev. Dynam.* **235**, 2603–2612.

**Nichols, D. H.** (1981). Neural crest formation in the head of the mouse embryo as observed using a new histological technique. *Development* **64**, 105–120.

**O'Rahilly, R. and Müller, F.** (2007). The development of the neural crest in the human. *J Anatomy* **211**, 335–351.

**Poelmann, R. E. and Gittenberger-de Groot, A. C.** (1999). A subpopulation of apoptosis-

prone cardiac neural crest cells targets to the venous pole: Multiple functions in heart development. *Developmental Biology* **207**, 271–286.

**Poh, Y.-C., Chen, J., Hong, Y., Yi, H., Zhang, S., Chen, J., Wu, D. C., Wang, L., Jia, Q., Singh, R., et al.** (2014). Generation of organized germ layers from a single mouse embryonic stem cell. *Nature Communications* **5**, 4000.

**Ralphs, J. R.** (1992). Chondrogenesis and myogenesis in micromass cultures of mesenchyme from mouse facial primordia. *In Vitro Cell. Dev. Biol.* **28A**, 369–372.

**Russ, A. P., Wattler, S., Colledge, W. H., Aparicio, S., Carlton, M., Pearce, J. J., Barton, S. C., Surani, M. A., Ryan, K., Nehls, M. C., et al.** (2000). Eomesodermin is required for mouse trophoblast development and mesoderm formation. *Nature* **404**, 95–99.

**Sakagami, N., Matsushita, Y., Syklawer-Howle, S., Kronenberg, H. M., Ono, W. and Ono, N.** (2018). Msx2 Marks Spatially Restricted Populations of Mesenchymal Precursors. *J. Dent. Res.* 22034518771014.

**Sauka-Spengler, T. and Bronner, M.** (2010). SnapShot: Neural Crest. *Cell* **143**, 486–486.

**Serbedzija, G. N., Bronner-Fraser, M. and Fraser, S. E.** (1989). A Vital Dye Analysis of the Timing and Pathways of Avian Trunk Neural Crest Cell-Migration. *Development* **106**, 809–816.

**Snippert, H. J. and Clevers, H.** (2011). Tracking adult stem cells. *EMBO Rep.* **12**, 113–122.

**Soriano, P.** (1999). Generalized lacZ expression with the ROSA26 Cre reporter strain. *Nat. Genet.* **21**, 70–71.

**Sperber, G. H., Sperber, S.M., Guttmann, G.D. and Tobias, P.V.** Craniofacial development. London: BC Decker, 2010.

**Trumpp, A., Depew, M. J., Rubenstein, J. L., Bishop, J. M. and Martin, G. R.** (1999). Cre-mediated gene inactivation demonstrates that FGF8 is required for cell survival and patterning of the first branchial arch. *Genes Dev.* **13**, 3136–3148.

**Underhill, T. M. and Weston, A. D.** (1998). Retinoids and their receptors in skeletal development. *Microsc. Res. Tech.* **43**, 137–155.

**Wales, M. M., Biel, M. A., Eldeiry, W., Nelkin, B. D., Issa, P., Cavenee, W. K., Kuerbitz, S. J. and Baylin, S. B.** (1995). P53 Activates Expression of Hic-1, a New Candidate Tumor-Suppressor Gene on 17p13.3. *Nat. Med.* **1**, 570–577.

**Wilkie, A. O. and Morriss-Kay, G. M.** (2001). Genetics of craniofacial development and malformation. *Nat Rev Genet* **2**, 458–468.

**Wright, E., Hargrave, M. R., Christiansen, J., Cooper, L., Kun, J., Evans, T., Gangadharan, U., Greenfield, A. and Koopman, P.** (1995). The Sry-related gene Sox9 is expressed during chondrogenesis in mouse embryos. *Nat. Genet.* **9**, 15–20.